

# Gaussian approximation for finitely extensible bead-spring chains with hydrodynamic interaction

R. Prabhakar\* and J. Ravi Prakash†

*Department of Chemical Engineering,  
Monash University, Clayton, Victoria - 3800,  
Australia*

(Dated: September 3, 2018)

The Gaussian Approximation, proposed originally by Öttinger [*J. Chem. Phys.*, 90 (1) : 463-473, 1989] to account for the influence of fluctuations in hydrodynamic interactions in Rouse chains, is adapted here to derive a new mean-field approximation for the FENE spring force. This FENE-PG force law approximately accounts for spring-force fluctuations, which are neglected in the widely used FENE-P approximation. The Gaussian Approximation for hydrodynamic interactions is combined with the FENE-P and FENE-PG spring force approximations to obtain approximate models for finitely-extensible bead-spring chains with hydrodynamic interactions. The closed set of ODE's governing the evolution of the second-moments of the configurational probability distribution in the approximate models are used to generate predictions of rheological properties in steady and unsteady shear and uniaxial extensional flows, which are found to be in good agreement with the exact results obtained with Brownian dynamics simulations. In particular, predictions of coil-stretch hysteresis are in quantitative agreement with simulations' results. Additional simplifying diagonalization-of-normal-modes assumptions are found to lead to considerable savings in computation time, without significant loss in accuracy.

## I. INTRODUCTION

The importance of hydrodynamic interactions (HI) in determining the behaviour of dilute polymer solutions has been widely recognized since the introduction of the Zimm theory<sup>1</sup>. The limitation, however, of the accuracy of Zimm theory to linear viscoelastic property predictions has spurred the development of more sophisticated treatments of HI. For instance, while the consistent averaging approximation<sup>2</sup> replaces the equilibrium averaged Oseen tensor in Zimm theory with a non-equilibrium average, the Gaussian approximation<sup>3,4</sup> further accounts for fluctuations in HI. The Gaussian approximation, which is the most sophisticated approximation to date, has been shown to be highly accurate in shear flows by comparing its predictions of viscometric functions with exact Brownian dynamics simulations (BDS)<sup>5</sup>.

The use of bead-spring chain models with linear Hookean springs in all these models has prevented the evaluation of their accuracy in extensional flows, in which the polymer coil undergoes a coil-stretch transition at a critical value  $Wi_c$  of the Weissenberg number  $Wi = \lambda \dot{\epsilon}$ , where  $\lambda$  is a characteristic relaxation time, and  $\dot{\epsilon}$  is the extension rate. As is well known, the extensional viscosity becomes unbounded at  $Wi_c$  because of the infinite extensibility of Hookean springs. The prediction of a bounded extensional viscosity was achieved in early theories by replacing Hookean springs with nonlinear finitely

extensible springs<sup>6</sup>. However, these theories did not incorporate HI. The important role played by HI in extensional flows has been established beyond doubt in a series of recent publications, which have shown that the inclusion of HI leads to quantitatively accurate predictions of both macroscopic and mesoscopic properties<sup>7,8,9,10,11</sup>. All these theoretical predictions have been obtained by carrying out exact BDS incorporating fluctuating HI and nonlinear finitely extensible springs.

An additional aspect that has been shown in these works to be crucial to obtaining quantitative predictions is the need to use bead-spring chain models with a sufficiently large number of springs,  $N_s$  (or equivalently, degrees of freedom). This requirement is eventuated by the need to accurately reflect both the changing nature of the drag experienced by the polymer as it unravels in an extensional flow, and the self-similar character of a high molecular weight polymer (which is responsible for the observation of universal behaviour in dilute polymer solutions). The requirement of large  $N_s$ , coupled with the need to include HI (which leads to the CPU time scaling as  $N_s^{4,5}$ ), makes the use of BDS for routine calculations highly impractical. While the development of schemes for the accelerated calculation of HI has alleviated this problem somewhat<sup>12</sup>, there is a pressing need for the development of approximations capable of describing extensional flows, that are both accurate and computationally inexpensive. The aim of this work is to introduce such an approximation by extending previous approximations for HI, which were based on bead-spring chain models with Hookean springs, to models with nonlinear finitely extensible springs.

Wedgewood and Öttinger<sup>13</sup> have previously introduced a similar approximation by combining the consistent av-

\*Present address: Research School of Chemistry, Australian National University, ACT - 0200, Australia

†Corresponding author

eraging scheme for HI with a FENE-P approximation for the springs. While they carried out a detailed investigation of the predictions of the model in shear flow, they did not evaluate its accuracy by comparison with exact BDS, nor did they obtain any predictions in extensional flows. In this work, we introduce an approximation that extends the previously established Gaussian approximation by accounting for fluctuations in *both* HI and the spring forces. The accuracy of this model is then verified by comparison with BDS in a number of both transient and steady, shear and extensional flows.

The reduction in computational time achieved by the introduction of such approximations, despite being significant, is not sufficient to explore the behaviour of truly long chains necessary to adequately model high molecular weight polymers. Several workers have shown that mapping the bead-connector vectors to ‘normal’ coordinates, followed by an assumption that certain matrices in the transformed space are diagonal, leads to further significant reductions in CPU time, without any sacrifice in accuracy<sup>14,15</sup>. Here, we carry out a similar diagonalization procedure, and examine both the reduction in CPU time, and its effect on the accuracy of the model.

The paper is organized as follows. In the following section, we recall the basic equations for non-free-draining bead-spring models of dilute solutions of finitely-extensible polymer molecules. Subsequently, we develop in section III, the equations for the Gaussian approximation, and its diagonalized version. Section IV introduces the flows and material functions of interest in this paper. The symmetries in the flow patterns considered lead to considerable simplifications in the implementation of the numerical methods for computing the material functions, which are briefly discussed in section V. Predictions of the approximations for the material functions in shear and extensional flows are presented in section VI along with the exact results obtained with BD simulations. Section VII summarizes the central conclusions of this study.

## II. BASIC EQUATIONS

Under homogeneous conditions, the configurational state of a bead-spring chain, with  $N_s$  springs, is completely specified by the set of connector vectors  $\{\mathbf{Q}_i \mid i = 1, \dots, N_s\}$ <sup>16</sup>. The Fokker-Planck equation governing the evolution of the configurational probability distribution  $\psi(\mathbf{Q}_1, \dots, \mathbf{Q}_{N_s}, t)$  is,

$$\begin{aligned} \frac{\partial \psi}{\partial t} = & - \sum_{i=1}^{N_s} \frac{\partial}{\partial \mathbf{Q}_i} \cdot \left\{ \boldsymbol{\kappa} \cdot \mathbf{Q}_i - \frac{1}{\zeta} \sum_{j=1}^{N_s} \tilde{\mathbf{A}}_{ij} \cdot \mathbf{F}_j^{s,c} \right\} \psi \\ & + \frac{k_B T}{\zeta} \sum_{i,j=1}^{N_s} \frac{\partial}{\partial \mathbf{Q}_i} \cdot \tilde{\mathbf{A}}_{ij} \cdot \frac{\partial \psi}{\partial \mathbf{Q}_j}, \end{aligned} \quad (1)$$

where,  $k_B$  is Boltzmann’s constant,  $\boldsymbol{\kappa}$  is the transpose of the position-independent traceless velocity gradient  $\nabla \mathbf{v}$ ,

$T$  is the absolute temperature of the solution, and  $\zeta$  is the Stokesian bead-friction coefficient, which is related to the bead radius  $a$  through  $\zeta = 6\pi a \eta_s$ , with  $\eta_s$  being the viscosity of the Newtonian solvent. The dimensionless diffusion tensors  $\tilde{\mathbf{A}}_{ij}$  are discussed in detail shortly. The spring connector force  $\mathbf{F}_j^{s,c}$  is given by,

$$\mathbf{F}_j^{s,c} = \frac{\partial S_j}{\partial \mathbf{Q}_j}, \quad (2)$$

with  $S_j$  representing the potential energy of spring  $j$ . Here, the following FENE expression for the spring force is used<sup>17</sup>:

$$\mathbf{F}_j^{s,c} = H \left( \frac{1}{1 - Q_j^2/Q_0^2} \right) \mathbf{Q}_j = H \xi(Q_j) \mathbf{Q}_j, \quad (3)$$

where,  $H$  is the spring constant,  $Q_j = |\mathbf{Q}_j|$ ,  $Q_0$  is the ‘fully-stretched’ length a single spring, and  $\xi = [1 - Q_j^2/Q_0^2]^{-1}$  is the nonlinearity in the FENE spring force law.

By considering a bead-spring chain of  $N_s$  springs to represent a polymer molecule of  $N_K$  Kuhn-segments, each spring can be imagined to represent a ‘sub-molecule’ of  $N_{K,s} = N_K/N_s$  Kuhn segments. The parameters in the FENE spring-force law,  $H$  and  $Q_0$ , can then be related to the two parameters characterizing the equilibrium structure of a sub-molecule, namely,  $b_K$  (the length of a Kuhn step) and  $N_{K,s}$ . Since the contour length of the sub-molecule is  $b_K N_{K,s}$ , it follows that  $Q_0 = b_K N_{K,s}$ . The equilibrium mean square end-to-end distance of a sub-molecule, in the absence of excluded volume forces, is  $R_s^2 = b_K^2 N_{K,s}$ . Using the equilibrium Boltzmann distribution for a single spring governed by the FENE spring force law,  $\psi_{\text{eq}}^s \sim \exp(-S_j/k_B T)$ , it can be shown that<sup>16</sup>,

$$\frac{H}{k_B T} = \frac{3}{R_s^2} - \frac{5}{Q_0^2}. \quad (4)$$

Substituting for  $R_s^2$  and  $Q_0^2$  in terms of  $b_K$  and  $N_{K,s}$ , leads to the following expression for the spring constant  $H$ ,

$$\frac{H}{k_B T} = \frac{1}{b_K^2} \frac{3N_{K,s} - 5}{N_{K,s}^2}. \quad (5)$$

The equations above indicate that taking the limit  $Q_0 \rightarrow \infty$ , while keeping  $R_s^2$  constant, leads to  $\xi \rightarrow 1$ . In this limit,  $R_s^2 = 3k_B T/H$ , and the FENE spring-force expression reduces to the Hookean spring force law,  $\mathbf{F}^{s,c} = H\mathbf{Q}$ . In this work, chains with Hookean springs are referred to as ‘Rouse’ chains, while finitely-extensible bead-spring chains are denoted as ‘FEBS’ chains.

The diffusion tensors  $\tilde{\mathbf{A}}_{ij}$  in Eq. (1) are given by,

$$\tilde{\mathbf{A}}_{ij} = A_{ij} \boldsymbol{\delta} + \zeta (\boldsymbol{\Omega}_{ij} + \boldsymbol{\Omega}_{i+1,j+1} - \boldsymbol{\Omega}_{i,j+1} - \boldsymbol{\Omega}_{i+1,j}), \quad (6)$$

where,  $A_{ij} = \delta_{ij} + \delta_{i+1,j+1} - \delta_{i,j+1} - \delta_{i+1,j} = 2\delta_{ij} - \delta_{|i-j|,1}$  is an element of the  $N_s \times N_s$  Rouse matrix, and

$\mathbf{\Omega}_{\nu\mu}$ ,  $\nu, \mu = 1, \dots, N$ , are HI tensors, which are typically related to the inter-bead displacement  $\mathbf{r}_{\mu\nu}$  between beads  $\mu$  and  $\nu$ , by expressions of the form,

$$\mathbf{\Omega}_{\nu\mu} = \frac{1}{8\pi\eta_s r_{\mu\nu}} \mathbf{C}(\mathbf{r}_{\mu\nu}). \quad (7)$$

Note that the inter-bead displacement vector  $\mathbf{r}_{\mu\nu}$  can be related to the spring connector vectors through,

$$\mathbf{r}_{\mu\nu} = \text{sgn}(\nu - \mu) \sum_{i=\min(\nu,\mu)}^{\max(\nu,\mu)-1} \mathbf{Q}_i. \quad (8)$$

Models which neglect the influence of HI—such as the original bead-spring model of Rouse<sup>18</sup>—can be interpreted as ones in which the tensor  $\mathbf{C}$  is set to zero. Early models incorporating HI<sup>1,19</sup> used the Oseen-Burgers form of the HI tensor, in which

$$\mathbf{C} = \boldsymbol{\delta} + \frac{\mathbf{r}_{\mu\nu}\mathbf{r}_{\mu\nu}}{r_{\mu\nu}^2}. \quad (9)$$

Although the Oseen-Burgers description of HI is inaccurate when the pair-wise separation between beads is comparable to the size of the beads, the hydrodynamic behaviour of long polymer chains is dominated by the interactions between non-adjacent beads, and the short-range inaccuracy of the Oseen-Burgers description has been shown to be relatively unimportant in the prediction of properties that depend on the polymer chain as a whole<sup>2,20</sup>.

Further, its simple form is particularly useful for the development of closure approximations. In numerical simulations, however, the Oseen-Burgers expression becomes problematic when  $r_{\nu\mu} \leq a$ , since the  $3N \times 3N$  diffusion block-matrix comprising the  $\tilde{\mathbf{A}}_{ij}$  tensors as its constituent blocks, can become non-positive definite<sup>21</sup> when beads overlap. In its place, in all the Brownian dynamics simulations performed here, the Rotne-Prager-Yamakawa (RPY) modification<sup>21,22</sup>,

$$\mathbf{C} = \begin{cases} \left(1 + \frac{2}{3} \frac{a^2}{r_{\mu\nu}^2}\right) \boldsymbol{\delta} + \left(1 - \frac{2a^2}{r_{\mu\nu}^2}\right) \frac{\mathbf{r}_{\mu\nu}\mathbf{r}_{\mu\nu}}{r_{\mu\nu}^2}, & r_{\mu\nu} \geq 2a, \\ \frac{r_{\mu\nu}}{2a} \left[ \left(\frac{8}{3} - \frac{3r_{\mu\nu}}{4a}\right) \boldsymbol{\delta} + \left(\frac{r_{\mu\nu}}{4a}\right) \frac{\mathbf{r}_{\mu\nu}\mathbf{r}_{\mu\nu}}{r_{\mu\nu}^2} \right], & r_{\mu\nu} < 2a. \end{cases} \quad (10)$$

which ensures that the diffusion block-matrix always remains positive-definite, is used.

In order to express the Fokker-Planck equation in dimensionless form, the following length scale and associated time scale are introduced<sup>9,10</sup>,

$$\ell_s \equiv \frac{R_s}{\sqrt{3}}; \quad \lambda_s \equiv \frac{\zeta \ell_s^2}{4k_B T}. \quad (11)$$

In the Hookean limit, both  $\ell_s$  and  $\lambda_s$  reduce to their conventional form,  $\ell_s = \ell_H = \sqrt{k_B T/H}$  and  $\lambda_s = \lambda_H =$

$\zeta/4H = \zeta \ell_H^2/4k_B T$ , respectively. Defining  $t^* \equiv t/\lambda_s$ ,  $\mathbf{Q}_i^* \equiv \mathbf{Q}_i/\ell_s$ ,  $\boldsymbol{\kappa}^* \equiv \lambda_s \boldsymbol{\kappa}$ , the Fokker-Planck equation can be recast in dimensionless terms as

$$\begin{aligned} \frac{\partial \psi}{\partial t^*} = & - \sum_{i=1}^{N_s} \frac{\partial}{\partial \mathbf{Q}_i^*} \cdot \left\{ \boldsymbol{\kappa}^* \cdot \mathbf{Q}_i^* - \frac{H^*}{4} \sum_{j=1}^{N_s} \tilde{\mathbf{A}}_{ij} \cdot \xi_j \mathbf{Q}_j^* \right\} \psi \\ & + \frac{1}{4} \sum_{i,j=1}^{N_s} \frac{\partial}{\partial \mathbf{Q}_i^*} \cdot \tilde{\mathbf{A}}_{ij} \cdot \frac{\partial \psi}{\partial \mathbf{Q}_j^*}, \end{aligned} \quad (12)$$

where,

$$H^* \equiv \frac{H \ell_s^2}{k_B T} = \frac{\ell_s^2}{\ell_H^2}, \quad (13)$$

is the dimensionless spring constant. When  $\ell_H$  is used as the length scale, the parameter  $Q_0$  is represented in dimensionless terms by the finite extensibility parameter,  $b \equiv Q_0^2/\ell_H^2$ . The counterpart of this parameter in the non-dimensionalization scheme adopted here is,  $b^* \equiv Q_0^2/\ell_s^2$ . Since  $Q_0 = b_{\kappa} N_{\kappa, s}$ , it follows that,  $b^* = 3N_{\kappa, s}$ . Because of the direct relation of  $b^*$  to the degree of coarse-graining  $N_{\kappa, s}$ , the latter is often reported instead of  $b^*$  when presenting results.

On introducing the hydrodynamic interaction parameter,  $h^*$ , defined by,

$$h^* = \frac{a}{\sqrt{\pi} \ell_s}, \quad (14)$$

the dimensionless tensor  $\zeta \mathbf{\Omega}_{\nu\mu}$  occurring in the definitions of the diffusion tensors [Eq. (6)] can be written as

$$\zeta \mathbf{\Omega}_{\nu\mu} = \frac{3\sqrt{\pi} h^*}{4 r_{\mu\nu}^*} \mathbf{C}(\mathbf{r}_{\mu\nu}^*), \quad (15)$$

where  $\mathbf{r}_{\mu\nu}^* = (1/\ell_s)\mathbf{r}_{\mu\nu}$ .

All the rheological properties of interest in the present work—which are discussed in greater detail in Section IV—can be obtained from Kramer's expression for the polymer contribution to the stress tensor  $\boldsymbol{\tau}_p$ <sup>16</sup>, which in non-dimensional terms is,

$$\boldsymbol{\tau}_p^* = \frac{1}{n_p k_B T} \boldsymbol{\tau}_p = N_s \boldsymbol{\delta} - H^* \sum_{i=1}^{N_s} \langle \xi_i \mathbf{Q}_i^* \mathbf{Q}_i^* \rangle. \quad (16)$$

Here,  $n_p$  is the number density of polymers,  $\boldsymbol{\delta}$  is the unit tensor, and angular brackets denote an average performed with the configurational distribution function  $\psi$ .

Besides rheological properties, the mean square end-to-end distance  $R_e^{*2}$  is used here to provide information on the size and shape of polymer molecules as they stretch and orient in response to the imposition of flow,

$$R_e^{*2} = \sum_{i,j=1}^{N_s} \text{tr} \langle \mathbf{Q}_i^* \mathbf{Q}_j^* \rangle. \quad (17)$$

Further, the prediction of the various models of the birefringence in extensional flows is evaluated using the following expression<sup>23,24</sup>:

$$\Delta n^* \equiv \frac{n_{xx}^I - n_{yy}^I}{A} = \frac{1}{b^*} \sum_{i=1}^{N_s} [\langle Q_{i,xx}^{*2} \rangle - \langle Q_{i,yy}^{*2} \rangle]. \quad (18)$$

where,  $\mathbf{n}^I$  is the intrinsic birefringence tensor, and  $A$  is a constant that, besides depending on the chemical structure of the polymer and the solvent, is proportional to the polymer concentration  $n_p$ .

Equations 16, 17 and 18 above show that all the macroscopic properties of interest here can be described in terms of expectations of configuration dependent functions. It is possible to obtain formally the equation for the time evolution of any configuration dependent function by multiplying the Fokker-Planck equation with the function and then integrating over all possible configurations. However, as a direct consequence of the nonlinearities in the model arising from FE and HI, the resulting equations are not closed with respect to the expectations whose evolution equations are desired. For instance, the following set of evolution equations for the second moments of the probability distribution  $\psi$  can be derived in this manner:

$$\begin{aligned} \langle \mathbf{Q}_i^* \mathbf{Q}_j^* \rangle_{(1)} &\equiv \frac{d\langle \mathbf{Q}_i^* \mathbf{Q}_j^* \rangle}{dt^*} - \boldsymbol{\kappa}^* \cdot \langle \mathbf{Q}_i^* \mathbf{Q}_j^* \rangle - \langle \mathbf{Q}_i^* \mathbf{Q}_j^* \rangle \cdot \boldsymbol{\kappa}^{*\text{T}} \\ &= -\frac{H^*}{4} \sum_{m=1}^{N_s} \langle \mathbf{Q}_i^* \mathbf{Q}_m^* \xi_m \cdot \tilde{\mathbf{A}}_{mj} + \tilde{\mathbf{A}}_{im} \cdot \xi_m \mathbf{Q}_m^* \mathbf{Q}_j^* \rangle \\ &\quad + \frac{1}{2} \langle \tilde{\mathbf{A}}_{ij} \rangle, \end{aligned} \quad (19)$$

where the subscript “(1)” denotes the contravariant convected time derivative of a tensor<sup>25</sup>. As a result of the nonlinearities in the functions  $\xi$  and  $\boldsymbol{\Omega}$  introduced by the spring force law and HI respectively, the equation above for  $\langle \mathbf{Q}_i^* \mathbf{Q}_j^* \rangle$  is not closed with respect to the second moments. It is this ‘closure problem’ that has motivated both the introduction of various closure schemes, and the development of exact Brownian dynamics simulations for obtaining predictions of properties away from equilibrium. As mentioned previously, the Gaussian approximation for Rouse chains is the most accurate closure approximation to date. In the section below, we develop the Gaussian approximation for FEBS chains with HI.

### III. GAUSSIAN APPROXIMATION

For Rouse chains, Öttinger<sup>3</sup> and Wedgewood<sup>4</sup> pointed out that the complicated averages on the right-hand side of equation 19 above (with  $\xi_m = 1$ ) can be expressed as functions of the second-moments  $\langle \mathbf{Q}_i^* \mathbf{Q}_j^* \rangle$  by *assuming a priori* that the configurational distribution function is

a multivariate Gaussian,

$$\psi = \mathcal{N} \exp \left[ -\frac{1}{2} \sum_{i,j=1}^{N_s} \mathbf{Q}_i^* \cdot \boldsymbol{\rho}_{ij}^* \cdot \mathbf{Q}_j^* \right], \quad (20)$$

where  $\mathcal{N}$  is a normalization factor. The tensors  $\boldsymbol{\rho}_{ij}^*$  are related to the second moments  $\boldsymbol{\sigma}_{ij}^* = \langle \mathbf{Q}_i^* \mathbf{Q}_j^* \rangle$  of the Gaussian distribution through the following set of  $N_s^2$  linear algebraic equations

$$\sum_{m=1}^{N_s} \boldsymbol{\sigma}_{im}^* \cdot \boldsymbol{\rho}_{mj}^* = \delta_{ij} \boldsymbol{\delta}. \quad (21)$$

As is well known, this implies that the Gaussian distribution  $\psi$  is completely specified once its second moments  $\boldsymbol{\sigma}_{ij}^*$  are known.

The crucial property of Gaussian distributions that enables the simplification of complex moments is described by Wick’s decomposition rule. In the present instance, because the right hand side of Eq. (19) has complex averages of the form  $\langle \mathbf{x} \mathbf{x} f(\mathbf{x}) \rangle$ , where  $\mathbf{x}$  is the random variable of interest, and  $f$  is a nonlinear function of  $\mathbf{x}$ , Wick’s decomposition rule leads to

$$\langle \mathbf{x} \mathbf{x} f \rangle = \langle \mathbf{x} \mathbf{x} \rangle \langle f \rangle + \langle \mathbf{x} \mathbf{x} \rangle \cdot \left\langle \frac{\partial f}{\partial \mathbf{x}} \right\rangle. \quad (22)$$

By applying Eq. 22 to Rouse chains with HI, Öttinger showed that Eq. (19) (with  $\xi_m = 1$ ) reduces to a closed set of equations for the second-moments  $\langle \mathbf{Q}_i^* \mathbf{Q}_j^* \rangle$ . In principle, the same approach can be used to obtain closure of Eq. (19) with both the nonlinear phenomena of finite extensibility and hydrodynamic interactions included. However, directly using the Gaussian assumption and Wick’s decomposition to simplify the expectations on the right-hand side of Eq. (19) leads to the incorrect prediction of a dependence of equilibrium static properties on  $h^*$ . Similar behaviour was earlier observed by Prabhakar and Prakash<sup>26</sup> when the Gaussian approximation was used to achieve closure in a Hookean dumbbell model simultaneously incorporating excluded volume and hydrodynamic interactions. The reason for this incorrect prediction is that, on direct application of the Gaussian approximation, the contributions from FE (and/or excluded volume) and those from HI cannot be separated into independent factors at equilibrium<sup>27</sup>, thus leading to an unphysical dependence of the predicted equilibrium second moments on the HI parameter,  $h^*$ . To avoid this problem, closure of Eq. (19) is achieved here in two steps. In the first step, a mean-field quadratic spring potential  $\bar{\mathcal{S}}_m^*$ , which approximately accounts for fluctuations in the FENE spring force, is derived by using the Gaussian approximation for *free-draining* FEBS chains. A bead-spring chain model is then constructed, which incorporates hydrodynamic interactions, and which has springs described by  $\bar{\mathcal{S}}_m^*$ . In the second step, the Gaussian approximation is again invoked to obtain a closed set of equations for the second moments of this model.

In this manner, the incorrect prediction of a dependence of equilibrium static properties on  $h^*$  is avoided.

Before discussing these two steps in detail in sections III.A and III.B below, it is appropriate to note that if  $f$  had been replaced with its average  $\langle f \rangle$  in Eq. 22, thus neglecting the fluctuations in  $f$ , one obtains the first term on the right-hand side alone. Thus, for a Gaussian distribution, it is seen that fluctuations in  $f$  are exactly accounted for by the second term on the right-hand side of the equation above. This convenient separation of the complicated expectation on the left hand side into contributions from the mean and fluctuations will be used here to highlight the important role played by fluctuations in the spring force and in hydrodynamic interactions.

### A. Free-draining FEBS chains

In this section, the Gaussian approximation is used to achieve closure of the second-moment equations for chains with finitely-extensible springs, but without HI. Prakash and co-workers have previously used the Gaussian approximation for bead-spring chain models without HI, but which are, however, still non-linear because of the presence of conservative non-hydrodynamic excluded volume forces between beads. The approximation was found by them to lead to qualitatively accurate predictions<sup>15,28,29,30</sup>.

For free-draining chains,  $\tilde{\mathbf{A}}_{ij} = A_{ij}\delta$ , and hence from Eq. (19), one obtains for FEBS chains

$$\begin{aligned} \langle \mathbf{Q}_i^* \mathbf{Q}_j^* \rangle_{(1)} &= -\frac{H^*}{4} \sum_{m=1}^{N_s} [\langle \mathbf{Q}_i^* \mathbf{Q}_m^* \xi_m \rangle A_{mj} + A_{im} \langle \xi_m \mathbf{Q}_m^* \mathbf{Q}_j^* \rangle] \\ &\quad + \frac{1}{2} A_{ij} \delta. \end{aligned} \quad (23)$$

The equation for the polymer stress is the same as in Eq. (16). In this case, closure of the evolution equation above is not possible because of the FENE nonlinearity,  $\xi_m$ , on the right-hand side. However, as in the case of the Gaussian approximation for HI, assuming that the configurational distribution is a Gaussian, and using Wick's decomposition rule, the problematic terms on the right-hand side of the equation above can be formally simplified. Since  $\partial S_m^*/\partial \mathbf{Q}_m^* = H^* \xi_m \mathbf{Q}_m^*$  (where,  $S_m^* = S_m/k_B T$ ), using Eq. (22) leads to

$$H^* \langle \mathbf{Q}_i^* \mathbf{Q}_m^* \xi_m \rangle = \left\langle \mathbf{Q}_i^* \frac{\partial S_m^*}{\partial \mathbf{Q}_m^*} \right\rangle = \sigma_{im}^* \cdot \left\langle \frac{\partial^2 S_m^*}{\partial \mathbf{Q}_m^* \partial \mathbf{Q}_m^*} \right\rangle \quad (24)$$

The expression on the right-hand side could have also been obtained by directly using a quadratic mean-field spring potential,

$$\bar{S}_m^* \equiv \frac{1}{2} \left\langle \frac{\partial^2 S_m^*}{\partial \mathbf{Q}_m^* \partial \mathbf{Q}_m^*} \right\rangle : \mathbf{Q}_m^* \mathbf{Q}_m^* \quad (25)$$

in place of the exact spring potential  $S_m^*$ . In other words, applying the Gaussian approximation to simplify the average due to FENE springs in free-draining chains is equivalent to using the quadratic mean-field spring potential  $\bar{S}_m^*$ , since this approximation leads to

$$\left\langle \mathbf{Q}_i^* \frac{\partial S_m^*}{\partial \mathbf{Q}_m^*} \right\rangle = \left\langle \mathbf{Q}_i^* \frac{\partial \bar{S}_m^*}{\partial \mathbf{Q}_m^*} \right\rangle \quad (26)$$

Prakash<sup>15</sup> have previously shown that Fixman's treatment of the excluded volume interaction potential<sup>31</sup> corresponds to the use of a similar pair-wise mean-field quadratic excluded volume potential.

The expression for  $\bar{S}_m^*$  in Eq. 25 can be simplified by using  $\partial S_m^*/\partial \mathbf{Q}_m^* = H^* \xi_m \mathbf{Q}_m^*$ ,

$$\bar{S}_m^* = H^* \left[ \langle \xi_m \rangle \delta + \left\langle \frac{\partial \xi_m}{\partial \mathbf{Q}_m^*} \mathbf{Q}_m^* \right\rangle \right] : \mathbf{Q}_m^* \mathbf{Q}_m^*. \quad (27)$$

The first term within the brackets on the right-hand side of the equation above containing  $\langle \xi_m \rangle$ , the average of the spring force nonlinearity, can be recognized as that arising from a consistent-averaging treatment of that nonlinearity, while the remaining term accounts for the influence of fluctuations in the spring force.

Recursive application of Wick's decomposition rule, using the result  $\partial \xi_m / \partial \mathbf{Q}_m^* = 2 \mathbf{Q}_m^* d\xi_m / d(Q_m^{*2})$ , leads to a series expansion,

$$\bar{S}_m^* = H^* \left[ \langle \xi_m \rangle \delta + \sum_{s=1}^{\infty} 2^s \left\langle \frac{d^s \xi_m}{d(Q_m^{*2})^s} \right\rangle \sigma_{mm}^{*s} \right] : \mathbf{Q}_m^* \mathbf{Q}_m^*, \quad (28)$$

where  $\sigma_{mm}^{*s}$  denotes the matrix product of  $s$  copies of  $\sigma_{mm}^*$ . The expansion above is valid provided the Gaussian averages  $\langle \xi_m \rangle$  and  $\langle d^s \xi_m / d(Q_m^{*2})^s \rangle$  exist for all  $s = 1, \dots, \infty$ . For FENE springs, however,

$$\xi_m = \frac{1}{(1 - Q_m^{*2}/b^*)}, \quad (29)$$

and,

$$\frac{d^s \xi_m}{d(Q_m^{*2})^s} = \frac{s!}{b^{*s}} \frac{1}{(1 - Q_m^{*2}/b^*)^{s+1}}. \quad (30)$$

The Gaussian averages of these functions do not exist since all of them have non-integrable singularities at  $Q_m^{*2} = b^*$ , whereas the Gaussian distribution has an infinite range. To make analytical progress, it is necessary to introduce further approximations. Here, analogous to the Peterlin closure approximation<sup>6</sup>,

$$\langle \xi_m \rangle \text{ is replaced with } \frac{1}{\langle (1 - Q_m^{*2}/b^*) \rangle} \quad (31)$$

and,

$$\left\langle \frac{d^s \xi_m}{d(Q_m^{*2})^s} \right\rangle \text{ is replaced with } \frac{s!}{b^{*s} \langle (1 - Q_m^{*2}/b^*)^{s+1} \rangle}. \quad (32)$$

Although each of these terms may remain bounded as long as  $\langle Q_m^{*2} \rangle = \text{tr } \boldsymbol{\sigma}_{mm}^* < b^*$ , there is a need to carefully analyze the convergence properties of the infinite series in Eq. (28) after introducing these approximations. Here, only the first term in the infinite series in Eq. (28) is retained to represent spring force fluctuations. As a result, the following mean-field quadratic spring potential

$$\begin{aligned} \mathbf{L}_m &\equiv \frac{1}{\langle (1 - Q_m^{*2}/b^*) \rangle} \boldsymbol{\delta} + \frac{2}{b^*} \frac{1}{\langle (1 - Q_m^{*2}/b^*)^2 \rangle} \boldsymbol{\sigma}_{mm}^* , \\ &= \frac{1}{1 - \text{tr } \boldsymbol{\sigma}_{mm}^*/b^*} \boldsymbol{\delta} + \frac{2/b^*}{1 - 2 \text{tr } \boldsymbol{\sigma}_{mm}^*/b^* + [(\text{tr } \boldsymbol{\sigma}_{mm}^*)^2 + 2 \boldsymbol{\sigma}_{mm}^* : \boldsymbol{\sigma}_{mm}^*]/b^{*2}} \boldsymbol{\sigma}_{mm}^* . \end{aligned} \quad (34)$$

The use of this potential leads to a reduction of the complex moments in Eq. 23,

$$H^* \langle \mathbf{Q}_i^* \mathbf{Q}_m^* \boldsymbol{\xi}_m \rangle = H^* \boldsymbol{\sigma}_{im}^* \cdot \mathbf{L}_m , \quad (35)$$

and a mean-field spring force given by,

$$\overline{\mathbf{F}}_m^{s,c} = H^* \mathbf{L}_m \cdot \mathbf{Q}_m^* . \quad (36)$$

As mentioned above, neglecting the spring force fluctuation term in  $\mathbf{L}_m$  is equivalent to a consistent-averaging treatment of the FENE nonlinearity, which leads to the well known FENE-P force law proposed originally by Bird *et al.*<sup>32</sup>,

$$\overline{\mathbf{F}}_m^{s,c} = H^* \frac{1}{1 - \text{tr } \boldsymbol{\sigma}_{mm}^*/b^*} \mathbf{Q}_m^* = H^* \bar{\boldsymbol{\xi}}_m \mathbf{Q}_m^* \quad (37)$$

where,  $\bar{\boldsymbol{\xi}}_m = [1 - \text{tr } \boldsymbol{\sigma}_{mm}^*/b^*]^{-1}$ . Incorporation of fluctuations through the Gaussian approximation leads to the spring force expression in Eq. (36), denoted here as the ‘‘FENE-PG’’ spring force law.

The evolution equation for the second moments in the Gaussian approximation for free-draining FEBS chains is consequently

$$\begin{aligned} \boldsymbol{\sigma}_{ij, (1)}^* &= -H^* \frac{1}{4} \sum_{m=1}^{N_s} (\boldsymbol{\sigma}_{im}^* \cdot \mathbf{L}_m A_{mj} + A_{im} \mathbf{L}_m \cdot \boldsymbol{\sigma}_{mj}^*) \\ &\quad + \frac{1}{2} A_{ij} \boldsymbol{\delta} , \end{aligned} \quad (38)$$

and the polymer stress predicted by the approximation is given by

$$\boldsymbol{\tau}_p^* = N_s \boldsymbol{\delta} - H^* \sum_{i=1}^{N_s} \boldsymbol{\sigma}_{ii}^* \cdot \mathbf{L}_i . \quad (39)$$

It is worth noting that for finite  $\boldsymbol{\sigma}_{mm}^*$ , as  $b^* \rightarrow \infty$ , the fluctuation contribution in Eq. (34) becomes vanishingly

is used,

$$\overline{\mathbf{S}}_m^* = \frac{H^*}{2} \mathbf{L}_m : \mathbf{Q}_m^* \mathbf{Q}_m^* , \quad (33)$$

where,

small,  $\mathbf{L}_m \rightarrow \boldsymbol{\delta}$  and the spring becomes more Hookean-like. On the other hand, as the bead-spring chain approaches its full extension, and

$$\boldsymbol{\sigma}_{mm}^* \rightarrow \begin{pmatrix} b^* & 0 & 0 \\ 0 & 0 & 0 \\ 0 & 0 & 0 \end{pmatrix} , \quad (40)$$

the scalar prefactor in the fluctuation term in Eq. (34) approaches  $(1/b^*)$ , which however becomes negligible compared to the FENE-P contribution, which diverges. Thus, as chains become highly stretched, predictions obtained with the FENE-P or FENE-PG approximations are expected to be nearly identical.

Although the FENE-PG approximation is new and has been developed in this study, the FENE-P approximation has been studied in great detail by several workers<sup>3,33,34,35,36,37,38,39</sup>. As pointed out in many of these studies, perhaps the single most important difference between the exact FENE and the mean-field FENE-P and FENE-PG approximations lies in the nature of the configurational probability distribution function. The singularity in the non-averaged FENE spring force strictly restricts the lengths of the connector vectors to lie in the domain  $[0, Q_0)$ . However, with the Peterlin closure, the solution of the modified Fokker-Planck equation with FENE-P/PG springs is a Gaussian. Therefore, there is a non-zero probability that a spring has a length greater than  $Q_0$ . This has been clearly illustrated by Keunings<sup>36</sup> who used Brownian dynamics simulations of dumbbells with FENE-P springs to show that in strong extensional flows, a significant proportion of the dumbbells had length greater than the ‘‘maximum allowed’’ dimensionless extension  $Q_0$ . However, in all the literature on the FENE-P model, the mean-squared lengths of the springs are observed to always be lesser than  $Q_0^2$ . In other words, the mean-field FENE-P model appears to satisfy the maximum extension constraint in an average sense.

It is observed in the studies cited above that predictions with the FENE-P approximation compare well with

the FENE model for steady-state properties, in both shear and uniaxial extensional flows. An explanation for the good agreement at steady-state in a strong flows is based on the observation that under such conditions most of the springs in the chain are highly stretched. The exact steady-state distribution function for the length of the spring in a dumbbell model is sharply peaked around  $\sqrt{\langle Q^2 \rangle}$ , and can be well approximated by a  $\delta$ -function<sup>34,40</sup>. However, during start-up of shear and extensional flows, predictions with the FENE-P model for the transient rheological properties deviate strongly from the exact results of BD simulations prior to the attainment of the steady-state<sup>37,38</sup>.

There have been several previous attempts to improve the FENE-P approximation. In conditions where springs can be highly stretched, the true spring length distribution is better approximated as the sum of a uniform distribution for smaller values of  $Q$  and a  $\delta$ -function located at a large  $Q$  closer to (but less than)  $Q_0$ . This FENE-L approximation, and its three-dimensional counterpart, are shown to be more accurate than the FENE-P model, particularly in predicting the phenomenon of stress-conformational hysteresis<sup>40,41,42</sup>. Grban *et al.*<sup>43</sup> show that an entropic argument can be used to improve upon the FENE-P approximation by first expanding the exact FENE potential in a Taylor's series expansion about  $\langle Q^2 \rangle$  and then systematically regrouping terms in the series before truncating it. This approach gives rise to a hierarchy of spring potentials of increasing complexity, the simplest of which is shown to be the quadratic potential corresponding to the FENE-P force law. By using the next higher order potential (which is denoted as the "FENE-P+1" potential by Gorban *et al.*) in the hierarchy, these authors demonstrate with a one-dimensional dumbbell model that accuracy is significantly improved in an unsteady elongational flow. In Section VI below, the accuracy of the FENE-PG model proposed in this study is evaluated by comparison with exact Brownian dynamics simulations.

The choice of parameter values  $H^*$  and  $b^*$  for the approximate FENE-P and FENE-PG models is made here consistently with the procedure used in the case of the FENE force law; namely, the equilibrium mean square end-to-end distance of a spring predicted by the model is equated to  $b_K^2 N_{K,s}$ , while the fully stretched length is equated to  $b_K N_{K,s}$ . Further, as before,  $\ell_s^2 = R_s^2/3 = b_K^2 N_{K,s}/3$ , and the corresponding time scale  $\lambda_s$ , are used as the basic scales for obtaining equations and properties in dimensionless form. These assumptions lead to  $b^* = Q_0^2/\ell_s^2 = 3N_{K,s}$ , as in the earlier case. From Eq. (38), it is clear that the equilibrium second moments  $\sigma_{ij,eq}^*$  predicted by the Gaussian approximation for free-draining FEBS chains, are solutions to the following set

of algebraic equations:

$$\mathbf{0} = -\frac{H^*}{4} \sum_{m=1}^{N_s} (\sigma_{im,eq}^* \cdot \mathbf{L}_{m,eq} A_{mj} + A_{im} \mathbf{L}_{m,eq} \cdot \sigma_{mj,eq}^*) + \frac{1}{2} A_{ij} \boldsymbol{\delta}. \quad (41)$$

At equilibrium, since  $\sigma_{ij,eq}^* = \sigma_{ij,eq}^* \boldsymbol{\delta}$  and  $\mathbf{L}_{m,eq} = L_{m,eq} \boldsymbol{\delta}$ , the equation above can be rearranged into the following set of equations,

$$0 = \sum_{m=1}^{N_s} (U_{im} A_{mj} + A_{im} U_{mj}) \quad (42)$$

where,

$$U_{ij} \equiv H^* \sigma_{ij,eq}^* L_{j,eq} - \delta_{ij} \quad (43)$$

Since the Rouse matrix is non-singular, the solution to Eq. (42) is obtained by setting  $U_{ij} = 0$ . This implies,  $\sigma_{ij,eq}^* = \delta_{ij} \boldsymbol{\delta}$ , and  $H^* \mathbf{L}_{j,eq} = \boldsymbol{\delta}$ . With all springs being identical at equilibrium,  $\mathbf{L}_{j,eq} = L_{eq} \boldsymbol{\delta}$ , and therefore

$$H^* L_{eq} = 1. \quad (44)$$

Using  $\text{tr} \sigma_{jj,eq}^* = 3$ , and  $b^* = 3N_{K,s}$ , it can be shown using Eq. (34) that for FENE-PG springs,

$$H^* = \frac{3N_{K,s}^3 - 9N_{K,s}^2 + 13N_{K,s} - 5}{3N_{K,s}^3 - 4N_{K,s}^2 + 5N_{K,s}}. \quad (45)$$

For FENE-P springs,  $L_{eq} = \bar{\xi}_{m,eq}$  (for all  $m$ ), where  $\bar{\xi}_m$  was introduced in Eq. (37) earlier. As a result,

$$H^* = \frac{1}{\bar{\xi}_{m,eq}} = 1 - \frac{1}{N_{K,s}}. \quad (46)$$

## B. FEBS chains with HI

The dimensionless evolution equation for the second-moments of a bead-spring chain model with springs obeying a mean-field potential given by Eq. (25), and with fluctuating HI between the beads, is given by,

$$\begin{aligned} \langle \mathbf{Q}_i^* \mathbf{Q}_j^* \rangle_{(1)} &= -\frac{H^*}{4} \sum_{m=1}^{N_s} \langle \mathbf{Q}_i^* \mathbf{Q}_m^* \cdot \mathbf{L}_m \cdot \tilde{\mathbf{A}}_{mj} \\ &+ \tilde{\mathbf{A}}_{im} \cdot \mathbf{L}_m \cdot \mathbf{Q}_m^* \mathbf{Q}_j^* \rangle + \frac{1}{2} \langle \tilde{\mathbf{A}}_{ij} \rangle, \end{aligned} \quad (47)$$

Since the tensors  $\mathbf{L}_m$  are not direct functions of the connector vectors, expectations of the form  $\langle \mathbf{Q}_i^* \mathbf{Q}_m^* \cdot \mathbf{L}_m \cdot (\zeta \boldsymbol{\Omega}_{mj}) \rangle$  appearing in the equation can be simplified by assuming that the configurational distribution function is Gaussian and using Wick's decomposition rule as in the

case of free-draining FEBS chains above. The final equation thus obtained for the approximate second-moments  $\sigma_{ij}^*$  is,

$$\begin{aligned} \sigma_{ij, (1)}^* = & -\frac{H^*}{4} \sum_{m=1}^{N_s} [\sigma_{im}^* \cdot (\mathbf{L}_m \cdot \bar{\mathbf{A}}_{mj} + \mathbf{\Delta}_{mj}) \\ & + (\bar{\mathbf{A}}_{im} \cdot \mathbf{L}_m + \mathbf{\Delta}_{mi}^T) \cdot \sigma_{mj}^*] + \frac{1}{2} \bar{\mathbf{A}}_{ij}, \end{aligned} \quad (48)$$

where, the tensor  $\bar{\mathbf{A}}_{ij}$  describes contributions arising from averaging the Oseen-Burgers tensor with the non-equilibrium distribution function, while the tensor  $\mathbf{\Delta}_{ij}$  represents contributions due to fluctuations in HI. Since the expressions for these tensors are lengthy and not very illuminating in themselves, they are given by Eqs. (A1) and (A2) in Appendix A. The important point to note

here is that  $\bar{\mathbf{A}}_{ij}$  and  $\mathbf{\Delta}_{ij}$  are completely expressible in terms of the second moments of the Gaussian distribution, and Eq. (48) is closed with respect to the tensors  $\sigma_{ij}^*$ .

At equilibrium, all the tensorial quantities in the equations above are isotropic. Furthermore, the HI fluctuation tensors  $\mathbf{\Delta}_{ij}$  vanish under isotropic conditions (see Appendix A). Consequently, one obtains an equation of the same form as Eq. (42):

$$0 = \sum_{m=1}^{N_s} [U_{im} \tilde{A}_{mj} + \tilde{A}_{im} U_{mj}], \quad (49)$$

in which the values of  $U_{ij}$  are the same as in Eq. (43) for the *free-draining* model with FENE-PG springs, and  $\tilde{A}_{im}$  are elements of the modified Rouse matrix (Eq. (50)),

$$\langle \tilde{A}_{ij} \rangle_{\text{eq}} = \tilde{A}_{ij} \boldsymbol{\delta} = \left[ A_{ij} + \sqrt{2} h^* \left( \frac{2}{\sqrt{|i-j|}} - \frac{1}{\sqrt{|i-j+1|}} - \frac{1}{\sqrt{|i-j-1|}} \right) \right] \boldsymbol{\delta}, \quad (50)$$

where, the convention  $1/\sqrt{0} = 0$  has been used. Since the modified Rouse matrix is also non-singular, the equilibrium solution is once again obtained by setting  $U_{ij} = 0$ . Therefore, the equilibrium solution obtained for the Gaussian approximation for FENE-PG chains with HI is identical to that obtained for free-draining FENE-PG chains. In other words, the heuristic two-step procedure outlined above to achieve closure in the model combining both FE and HI ensures that the equilibrium solution for the second-moments is independent of HI.

Nearly all the closure approximations introduced to date for the second-moments  $\langle \mathbf{Q}_i^* \mathbf{Q}_j^* \rangle$  can be derived by dropping appropriate terms in Eq. (48). For instance, the Zimm model is obtained by (i) using a Hookean spring force law,  $\mathbf{L}_m = \boldsymbol{\delta}$ , (ii) replacing the non-equilibrium averaged Oseen tensor contribution  $\bar{\mathbf{A}}_{ij}$  with the modified Rouse matrix  $\tilde{A}_{ij}$  (which arises due to equilibrium averaging the Oseen tensor), and (iii) setting  $\mathbf{\Delta}_{ij} = \mathbf{0}$ . Ignoring fluctuations in hydrodynamic interactions in a model with Hookean springs ( $\mathbf{\Delta}_{ij} = \mathbf{0}$  and  $\mathbf{L}_m = \boldsymbol{\delta}$ ) leads to the consistent averaging (CA) approximation<sup>2</sup>, while retaining fluctuations in HI leads to the Gaussian approximation (GA)<sup>3</sup>. Setting  $\mathbf{\Delta}_{ij} = \mathbf{0}$  and  $\mathbf{L}_m = \bar{\xi}_m \boldsymbol{\delta}$  simultaneously (which implies fluctuations in both HI and the spring force are ignored), leads to a model combining the Consistent-Averaging treatment of HI with the FENE-P approximation for the spring force. The predictions of this CA-P model for properties in shear flows have been studied in detail by Wedgewood and Öttinger<sup>13</sup>. On the other hand, using only one of the two conditions leads to a model in which fluctuations in the corresponding phenomenon alone are ignored, leading to the CA-PG model

TABLE I Acronyms used for referring to approximate models.

Acronym	
Treatment of HI	
Free-draining	FD
Equilibrium-averaging	EA
Consistent-averaging	CA
Gaussian approximation	GA
Treatment of FE	
Hookean springs	H
FENE-P	P
FENE-PG	PG

or the GA-P model. The model incorporating fluctuations in both nonlinear phenomena is referred to here as the GA-PG model. Note that in all these models, the polymer stress is given by Eq. (39), with the appropriate choice of  $\mathbf{L}_i$ .

In discussing predictions obtained using the various approximate models, it is convenient to use acronyms in which the first two letters refer to the approximation used for HI, and the last letters refer to that used for FE. Table I lists the letter codes used for easy reference. Note that in this scheme, the Rouse model is denoted as the FD-H model, while the Zimm model is denoted as EA-H.

### C. Diagonalization

Previous studies have shown that considerable savings in computational time, without a significant loss in accuracy, may be achieved by introducing a *diagonalization approximation*<sup>14,44</sup>. The most recent of these approximations, carried out in the context of the Gaussian approximation for Rouse chains with HI, is the ‘‘Two-Fold Normal’’ (TFN) approximation of Prakash and Öttinger<sup>44</sup> (named as such because of two different assumptions of ‘‘normality’’—a Normal distribution, and a transformation to normal coordinates). Prakash and Öttinger showed that for Rouse chains with HI, the predictions of the TFN approximations for linear viscoelastic properties and steady-state material functions in shear are close to those obtained with the original Gaussian approximation. Here, we examine the effectiveness of making a similar approximation for FENE-P chains with HI.

The first step in introducing a diagonalization approximation is mapping the set of the physical connector vectors  $\{\mathbf{Q}_i^* | i = 1, \dots, N_s\}$  onto a set of normal coordinates  $\{\mathbf{Q}'_p | p = 1, \dots, N_s\}$  using the following transformation,

$$\mathbf{Q}'_p = \sum_{i=1}^{N_s} \Pi_{ip}^Z \mathbf{Q}_i^*, \quad (51)$$

where  $\Pi_{ip}^Z$  are the elements of the orthogonal matrix whose columns are formed by the eigenvectors of the modified Rouse matrix,

$$\sum_{i,j=1}^{N_s} \Pi_{ip}^Z \tilde{A}_{ij} \Pi_{jq}^Z = \delta_{pq} \tilde{a}_p, \quad (52)$$

in which  $\tilde{a}_p$  is an eigenvalue of the modified Rouse matrix. The orthogonal matrix corresponding to the Rouse matrix is used for free-draining models without HI, for effecting the transformation to normal coordinates. Using the orthogonality relation

$$\sum_{k=1}^{N_s} \Pi_{mk}^Z \Pi_{nk}^Z = \delta_{mn} = \sum_{k=1}^{N_s} \Pi_{km}^Z \Pi_{kn}^Z, \quad (53)$$

the evolution equations for the covariances of the normal coordinates  $\boldsymbol{\sigma}'_{pq}$  defined as,

$$\boldsymbol{\sigma}'_{pq} = \sum_{i,j=1}^{N_s} \Pi_{ip}^Z \boldsymbol{\sigma}_{ij}^* \Pi_{jq}^Z, \quad (54)$$

can be shown to be,

$$\begin{aligned} \boldsymbol{\sigma}'_{pq,(1)} = & -\frac{1}{4} \sum_{u=1}^{N_s} [\boldsymbol{\sigma}'_{pu} \cdot (\mathbf{X}_{uq} + \mathbf{Y}_{uq}) + (\mathbf{X}_{up} + \mathbf{Y}_{up}^T) \cdot \boldsymbol{\sigma}'_{uq}] \\ & + \frac{1}{2} \mathbf{Z}_{pq}, \end{aligned} \quad (55)$$

where the auxiliary tensors are defined by,

$$\mathbf{Z}_{pq} \equiv \sum_{i,j=1}^{N_s} \Pi_{ip}^Z \bar{\mathbf{A}}_{ij} \Pi_{jq}^Z, \quad (56)$$

$$\mathbf{X}_{pq} \equiv H^* \sum_{i,j=1}^{N_s} \Pi_{ip}^Z \bar{\xi}_i \bar{\mathbf{A}}_{ij} \Pi_{jq}^Z, \quad (57)$$

$$\mathbf{Y}_{pq} \equiv H^* \sum_{i,j=1}^{N_s} \Pi_{ip}^Z \bar{\xi}_i \boldsymbol{\Delta}_{ij} \Pi_{jq}^Z. \quad (58)$$

Following Prakash and Öttinger, we *assume* that the normal coordinates covariance matrix is diagonal,

$$\boldsymbol{\sigma}'_{pq} \approx \delta_{pq} \boldsymbol{\sigma}'_p, \quad (59)$$

This leads to the following set of equations for the normal coordinate variances,

$$\boldsymbol{\sigma}'_{p,(1)} = -\frac{1}{4} [\boldsymbol{\sigma}'_p \cdot (\mathbf{X}_p + \mathbf{Y}_p) + (\mathbf{X}_p + \mathbf{Y}_p^T) \cdot \boldsymbol{\sigma}'_p] + \frac{1}{2} \mathbf{Z}_p, \quad (60)$$

where the notation  $(\dots)_p = (\dots)_{pp}$  is used. While Prakash and Öttinger argue that it is not necessary to make the additional diagonalization assumptions,

$$\mathbf{Z}_{pq} \approx \mathbf{Z}_p \delta_{pq}; \quad \mathbf{X}_{pq} \approx \mathbf{X}_p \delta_{pq}; \quad \mathbf{Y}_{pq} \approx \mathbf{Y}_p \delta_{pq} \quad (61)$$

in order to derive Eq. (60), Eq. (55) shows that for the time derivatives of the off-diagonal components of the normal-mode covariances to remain negligible far from equilibrium, it is necessary for both Eq. (59) and Eqs. (61) to be true.

Equation (60) represents a set of  $N_s$  ODE's that are coupled and nonlinear. The coupling comes about because the auxiliary tensors  $\mathbf{Z}_p$ ,  $\mathbf{X}_p$  and  $\mathbf{Y}_p$  depend on all the variances  $\boldsymbol{\sigma}_{ij}^*$ . For instance, the FENE-P factors appearing in these terms are evaluated as

$$\bar{\xi}_p = \frac{1}{1 - \left[ \sum_{p=1}^{N_s} \Pi_{pm}^{Z2} \text{tr}(\boldsymbol{\sigma}'_m) \right] / b^*}. \quad (62)$$

As a result of the coupling, the CPU-time per time step scales as  $N_s^3$ , even though the number of equations is only  $N_s$ . For every  $p$  in Eq. (60), each calculation of  $\mathbf{Z}_p$ ,  $\mathbf{X}_p$  and  $\mathbf{Y}_p$  individually involves a double summation over all  $i$  and  $j$  in Eqs. (56), (57) and (58). In the calculation of the variances  $\boldsymbol{\sigma}_{\mu\nu}^*$  using Eq. (A6), each of the  $\boldsymbol{\sigma}_{ij}^*$  requires a summation over all  $k$ , as can be seen from,

$$\boldsymbol{\sigma}_{ij}^* = \sum_{k=1}^{N_s} \Pi_{ik}^Z \boldsymbol{\sigma}'_k \Pi_{jk}^Z. \quad (63)$$

Since the values of  $\boldsymbol{\sigma}_{ij}^*$  can be stored at the beginning of each time-step, the total cost of generating the supermatrix containing the  $\boldsymbol{\sigma}_{ij}^*$  tensors scales as  $N_s^3$ . The cost

of the calculating  $\mathbf{S}_{\mu\nu}^*$  using

$$\mathbf{S}_{\mu\nu}^* = \mathbf{S}_{\mu,\nu-1}^* + \sum_{i=\mu}^{\nu-2} (\boldsymbol{\sigma}_{i,\nu-1}^* + \boldsymbol{\sigma}_{\nu-1,i}^*) + \boldsymbol{\sigma}_{\nu-1,\nu-1}^*, \quad \mu < \nu, \quad (64)$$

can also be shown to scale as  $N_s^3$ . Thus, as far as the CPU-time scaling is concerned, the diagonalization assumption does not offer an advantage over the original approximations in the calculation of properties in unsteady flows using bead-spring models with HI. However, the reduction in the number of equations to be integrated greatly reduces the prefactor in the CPU-time's power-law dependence on  $N_s$ , and as will be shown in section VI.C, leads to a significant reduction in CPU time.

The diagonalized versions of the models will be referred to with a ‘‘D’’ prefixed to the acronym representing the original approximation, *e.g.* DFD-P, DCA-P *etc.* The exception to this rule is the TFN-P model, combining the TFN approximation for HI with FENE-P springs.

Before presenting results, the next two sections briefly introduce the main material functions examined here, and the numerical schemes used to obtain them.

#### IV. MATERIAL FUNCTIONS

Attention is restricted here to some instances of simple shear and uniaxial extensional flows. Expressions for the material functions in these flows, in terms of components of the stress tensor, are discussed below.

##### A. Shear flow

For a simple homogeneous shear flow characterized by the shear rate  $\dot{\gamma}$ , the continuum solvent's velocity components in Cartesian coordinates are given by  $v_x = \dot{\gamma}(t)y$ ,  $v_y = 0$  and  $v_z = 0$ . The tensor  $\boldsymbol{\kappa}^* = \lambda_s \nabla \mathbf{v}$  in Cartesian coordinates is

$$\boldsymbol{\kappa}^*(t^*) = \dot{\gamma}^*(t^*) \begin{pmatrix} 0 & 1 & 0 \\ 0 & 0 & 0 \\ 0 & 0 & 0 \end{pmatrix}, \quad (65)$$

where  $\dot{\gamma}^*(t^*) = \dot{\gamma}(t)\lambda_s$  is the time dependent dimensionless shear rate. Here, the time dependence of solution properties is examined for the sudden imposition of steady shear flow:

$$\dot{\gamma}^*(t^*) = \begin{cases} 0, & t^* < 0, \\ \dot{\gamma}^*, & t^* \geq 0. \end{cases} \quad (66)$$

While the imposed strain rate  $\dot{\gamma}^*$  at  $t^* \geq 0$  is a constant, the solution as a whole is in an unsteady state since the properties of the solution change in response to the imposition of the flow. Steady-state is reached when all properties reach time-independent values which are

functions solely of the imposed strain rate and the other physical parameters characterizing the solution.

For a simple shear flow defined in Eq. (66), the rheological properties of interest are the polymer's contribution to the dimensionless viscosity  $\eta_p^*$ , the dimensionless first normal-stress difference coefficient  $\Psi_1^*$ , and the dimensionless second normal-stress difference coefficient  $\Psi_2^*$ , which are respectively defined by the following relations:

$$\eta_p^* \equiv -\frac{\tau_{p,yy}^*}{\dot{\gamma}^*}, \quad (67)$$

$$\Psi_1^* \equiv -\frac{\tau_{p,xx}^* - \tau_{p,yy}^*}{\dot{\gamma}^{*2}}, \quad (68)$$

$$\Psi_2^* \equiv -\frac{\tau_{p,yy}^* - \tau_{p,zz}^*}{\dot{\gamma}^{*2}}. \quad (69)$$

##### B. Extensional flow

In a uniaxial extensional flow with an extension-rate  $\dot{\varepsilon}$ , the velocity field is specified by  $v_x = \dot{\varepsilon}(t)x$ ,  $v_y = -(\dot{\varepsilon}(t)/2)y$  and  $v_z = -(\dot{\varepsilon}(t)/2)z$ . Therefore,

$$\boldsymbol{\kappa}^*(t^*) = \dot{\varepsilon}^*(t^*) \begin{pmatrix} 1 & 0 & 0 \\ 0 & -\frac{1}{2} & 0 \\ 0 & 0 & -\frac{1}{2} \end{pmatrix}, \quad (70)$$

where  $\dot{\varepsilon}^*(t^*) = \dot{\varepsilon}(t)\lambda_s$  is the time dependent dimensionless extension-rate. Here, the time dependence of solution properties is examined for the following kinds of unsteady extensional flows.

Sudden imposition of steady shear or uniaxial extensional flow:

$$\dot{\varepsilon}^*(t^*) = \begin{cases} 0, & t^* < 0, \\ \dot{\varepsilon}^*, & t^* \geq 0. \end{cases} \quad (71)$$

Sudden imposition followed by cessation of steady uniaxial extensional flow:

$$\dot{\varepsilon}^*(t^*) = \begin{cases} 0, & t^* < 0, \\ \dot{\varepsilon}^*, & 0 \leq t^* \leq t_{\max}^* \text{ (the stress-growth phase)}, \\ 0, & t^* > t_{\max}^* \text{ (the stress-relaxation phase)}. \end{cases} \quad (72)$$

The time-dependence of properties in an unsteady state is expressed in terms of the strain measure  $\epsilon = \dot{\varepsilon}^* t^*$ .

In the case of a uniaxial extensional flow specified by Eq. (71), the polymer contribution to the dimensionless extensional viscosity, denoted as  $\bar{\eta}_p^*$ , is given by

$$\bar{\eta}_p^* \equiv -\frac{\tau_{p,xx}^* - \tau_{p,yy}^*}{\dot{\varepsilon}^*}. \quad (73)$$

For the flow pattern described in Eq. (72), rheological data is presented in this work in terms of  $N_1^*$ , the magnitude of the polymer's contribution to the dimensionless

first normal stress difference:

$$N_{1,p}^* = |\tau_{p,xx}^* - \tau_{p,yy}^*|. \quad (74)$$

We note here that the characterization of a shear rate as “low” or “high”, depends on whether the Weissenberg number is much lower, or greater than unity. The Weissenberg number is defined as the product of the shear (or extension) rate and a time-scale characterizing the large scale dynamics of isolated chains near equilibrium. As is well known, this characteristic time-scale is proportional to  $N^2$  for free-draining chains, whereas in chains with HI, it is proportional to  $N^{3/2}$ . The Weissenberg number in these two cases thus scales as  $\dot{\gamma}^* N^2$  and  $\dot{\gamma}^* N^{3/2}$ , respectively. For  $N = 20$ , a shear rate of  $\dot{\gamma}^* \sim 1$  therefore represents a large strain rate, as will become evident in the results below. In extensional flows, the critical strain rate for the coil-to-stretch transition (discussed in section VI.B) marks the boundary between small and large extension rates.

## V. NUMERICAL METHOD

In the case of the un-diagonalized approximations, the total number of second moments, and therefore the number of equations, is equal to  $9N_s^2$ . However,  $\boldsymbol{\sigma}_{ij}^* = \boldsymbol{\sigma}_{ji}^{*\text{T}}$ . Further, the second moments must not change if the bead numbering is reversed. Thus,  $\boldsymbol{\sigma}_{ij}^* = \boldsymbol{\sigma}_{N_s-i, N_s-j}^*$ . Therefore, the number of independent second moments reduces by a factor of nearly  $1/4^3$ . In the diagonalized approximations, on the other hand, the number of equations for the components of the normal mode variances is just  $9N_s$ .

The symmetry of the imposed flow field can be used to reduce the number of components for all the tensorial quantities in the equations. In shear flows, the second moment tensors take the following form:

$$\boldsymbol{\sigma} = \begin{pmatrix} \sigma_1 & \sigma_4 & 0 \\ \sigma_5 & \sigma_2 & 0 \\ 0 & 0 & \sigma_3 \end{pmatrix}. \quad (75)$$

In uniaxial extensional flows, in both stress growth and relaxation phases, all tensorial quantities in the approximations have the form,

$$\boldsymbol{\sigma} = \begin{pmatrix} \sigma_1 & 0 & 0 \\ 0 & \sigma_2 & 0 \\ 0 & 0 & \sigma_2 \end{pmatrix}. \quad (76)$$

The exploitation of the symmetries above to reduce the computation of the fourth rank tensorial function  $\mathbf{K}(\mathbf{s})$  has been discussed thoroughly by Zylka<sup>5</sup>. In general, for any symmetric tensor  $\mathbf{s}$ , only 21 of the 81 components of the  $\mathbf{K}$  function are non-zero in a transformed coordinate system  $C$  in which the tensor  $\mathbf{s}$  has a diagonal representation. Out of these 21 components, only 9 require independent numerical evaluation. The components  $K_{1111}$ ,

$K_{2222}$  and  $K_{3333}$  can be used to calculate the remaining 12 non-zero components. Furthermore, the function  $\mathbf{K}$  always appears in the equations as  $\mathbf{K} : \boldsymbol{\sigma}$ . In shear flows, this means that only 14 components of the  $\mathbf{K}$  function in the laboratory fixed coordinate system are required to be evaluated. In uniaxial extensional flows, it can be shown that only  $K_{xxxx}$  (where  $x$  is the direction of stretching) is required. As shown by Zylka<sup>5</sup>, components of the  $\mathbf{H}(\mathbf{s})$  and  $\mathbf{K}(\mathbf{s})$  functions in the coordinate system  $C$  are efficiently evaluated using elliptic integrals.

The initial condition for the time integration of the ODE’s starting from equilibrium is  $\boldsymbol{\sigma}_{ij, \text{eq}}^* = \delta_{ij} \boldsymbol{\delta}$  for the un-diagonalized approximations. Similarly, in the case of the diagonalized approximations,

$$\boldsymbol{\sigma}'_{p, \text{eq}} = \sum_{i,j=1}^{N_s} \Pi_{ip}^z \boldsymbol{\sigma}_{ij, \text{eq}}^* \Pi_{jp}^z = \sum_{i,j=1}^{N_s} \Pi_{ip}^z (\delta_{ij} \boldsymbol{\delta}) \Pi_{jp}^z = \boldsymbol{\delta}. \quad (77)$$

As pointed out in the preceding sections, at equilibrium  $\bar{\mathbf{A}}_{ij, \text{eq}} = \tilde{A}_{ij} \boldsymbol{\delta}$ ,  $\Delta_{ij, \text{eq}} = \mathbf{0}$ ,  $H^* \mathbf{L}_{i, \text{eq}} = \boldsymbol{\delta}$ .

Since predictions are obtained only for shear and uniaxial extensional flows in this study, separate computer codes were written for the two different flows, to take advantage of the reduction in the components due to their individual flow symmetries. A variable-step Adams method (the D02CJF routine in the NAG library) is used for the integration of the ODE’s.

Steady-state solutions were obtained by setting the time derivatives in the ODE’s to zero, and then using a Wegstein successive substitution algorithm to solve the set of nonlinear equations. Solutions are obtained for several values of the (shear or extensional) strain rate. The converged solution for the set of  $\boldsymbol{\sigma}_{ij}^*$  (or  $\boldsymbol{\sigma}'_p$ ) at any strain rate is used as the initial guess for the next higher (or lower) strain rate for which a solution is desired. It is found that large steps in the strain rates could lead to unphysical, non-positive-definite solutions for the second moments<sup>13,14</sup>. Such behaviour is avoided by manually controlling the size of the steps in strain rate.

The Brownian dynamics simulations of Rouse and FENE chains with (and without) RPY-HI performed in this study use a modification of the semi-implicit predictor-corrector scheme outlined recently by several workers<sup>8,45,46</sup>, where the error between the predictor and corrector steps is used to adaptively control the time-step size in every simulation.

## VI. RESULTS AND DISCUSSION

Results for shear flows and extensional flows are discussed separately in the respective sections below. In each case, results are presented for (i) models with non-linear force laws, but with no HI, (ii) models with HI incorporated, but with a linear Hookean force law, and (iii) models with non-linear force laws and HI incorporated. In particular, in case (i), results obtained with

the new FENE-PG force law introduced here are compared with results obtained with the FENE-P force law and with BDS, in case (ii) (which involves only models that have been introduced previously), results for certain material functions that have not been predicted earlier, are presented, and in case (iii), the combined influence of both phenomena are examined, aided by the results obtained in cases (i) and (ii).

## A. Shear flow

### 1. Startup of shear flow

The performance of the FENE-P and FENE-PG approximations for free-draining FEBS chains in the prediction of unsteady behaviour in shear flows is first considered. At low shear rates close to equilibrium, finite chain extensibility has little influence on the dynamic behaviour predicted by the models. Therefore, the predictions of the free-draining FEBS models are close to those predicted with the Rouse model. At higher shear rates, earlier studies with free-draining FENE-P dumbbells<sup>37</sup> and chains with  $N = 10^{38}$  show that this approximation leads to predictions for unsteady shear properties that agree only qualitatively with the exact results obtained using FENE springs. Figures 1 (a) and (b) show that this trend is continued for 20-bead chains. The incorporation of fluctuations in the spring force with the use of the FENE-PG approximation leads to a clear improvement in the quality of the predictions for all properties at moderate shear rates (represented by the curves for  $\dot{\gamma}^* = 0.23$ ). As the dimensionless shear rate approaches unity, however, the FENE-PG approximation also begins to deviate from the exact BDS results. Interestingly, it is seen that the FENE-PG force law leads to the prediction of a transient non-zero positive second-normal stress difference which approaches zero at steady-state, in good agreement (within errors in the simulations' results) with the results of simulations.

A striking feature is the large overshoots predicted by all the models in the growth of  $\eta_p^*$  in Fig. 1 (a). A similar prediction is obtained for  $\Psi_1^*$ . This feature is not observed at any shear rate for Rouse chains with HI (see Fig. 2 (a)), and neither is it observed at low shear rates for FEBS chains. The overshoots in the material functions appear to be accompanied by a corresponding overshoot in the mean-squared end-to-end distance of the coils. Overshoots in the transient  $\eta_p^*$ ,  $\Psi_1^*$  and  $R_e^{*2}$  during start-up of shear flows are known to be a signature of the influence of FE<sup>37,38,47,48</sup>. Hur et al. have obtained experimental evidence of such overshoots using dilute (and semi-dilute) solutions of DNA, and have shown using simulations of bead-rod and bead-spring chains that the overshoot is caused by the rapid localized stretching of the molecules by the flow, before the orientation of the chains towards the flow direction reduces the total solvent drag sufficiently to reduce the stretching. Herrchen an

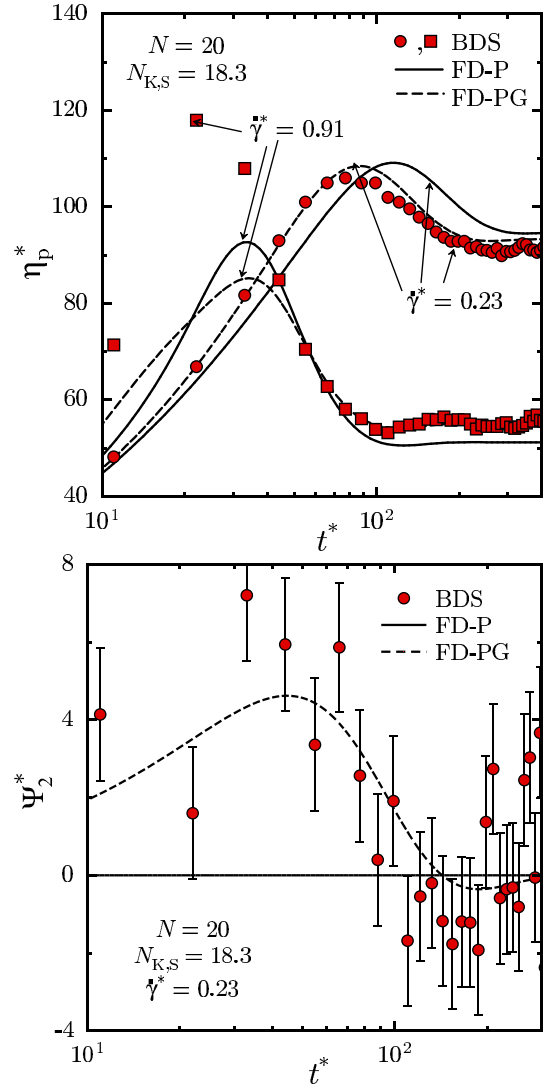


FIG. 1 Growth of (a) viscosity and (b) second normal-stress difference coefficient, for free-draining FEBS chains during start-up of steady shear flow.

döttinger<sup>37</sup> observed that the overshoot predicted with FENE-P springs is larger than that obtained with FENE springs in the case of dumbbells.

Although the qualitative behaviour of the different approximations for HI in Rouse chains has been well documented in the case of steady shear flows, their predictions of rheological and conformational properties in transient shear flows have not received much attention. For Rouse chains with HI, use of equilibrium averaging in the Zimm models results in a fixed time dependence of properties that is independent of the shear rate<sup>16</sup>. This behaviour parallels the shear rate independence of the material functions predicted at steady-state by the Zimm model. In contrast, the predictions of the consistent-averaging and Gaussian approximations, and the exact results of the simulations for the growth of the shear material functions depend on the imposed shear rate, as demonstrated

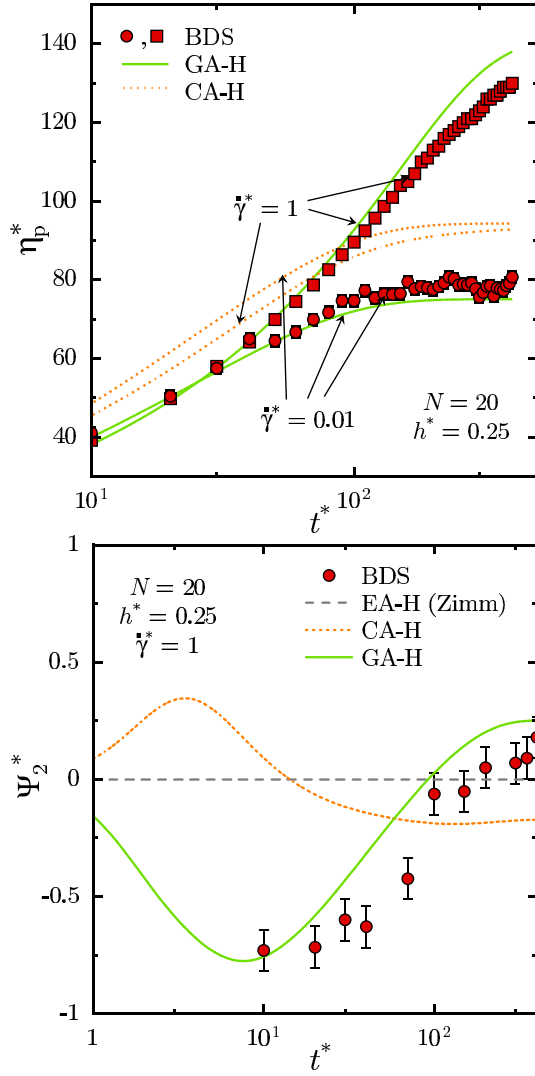


FIG. 2 Growth of (a) viscosity, and (b) second normal-stress difference coefficient, for Rouse chains with HI during start-up of steady shear flow.

in Figs. 2 (a) and (b) for the transient variation in  $\eta_p^*$  and  $\Psi_2^*$ , respectively, after the imposition of a steady shear rate.

In Fig. 2 (a), the curves predicted with the Gaussian approximation initially lie below those predicted with consistently averaged HI, for both the shear rates considered. At larger values of  $t^*$ , as steady-state is approached, the prediction of the Gaussian approximation at the higher shear rate is seen to overtake the CA-H curve, whereas at the lower shear rate, the GA-H prediction is always below that predicted by the CA-H model. The importance of including a description of the fluctuations in approximate models accounting for HI is clearly highlighted by the superiority of the predictions of the Gaussian approximation. Interestingly, Fig. 2 (b) shows that fluctuations in HI lead to a negative second normal stress difference coefficient soon after the inception of flow. Zylka<sup>5</sup> had earlier demonstrated the accurate pre-

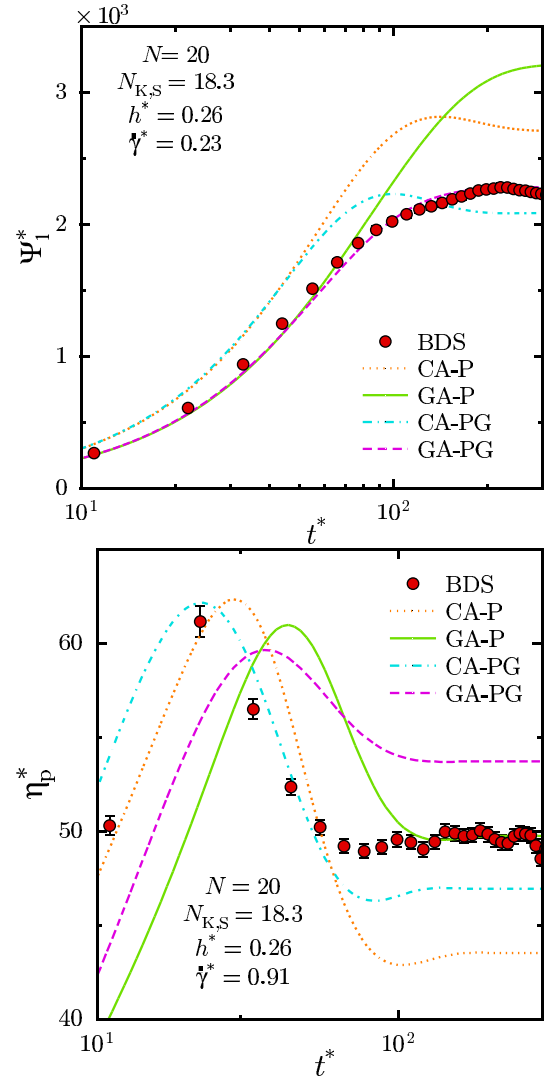


FIG. 3 Growth of (a) first normal-stress difference coefficient, and (b) viscosity, for FEBS chains with HI during start-up of steady shear flow.

diction of the sign of  $\Psi_2^*$  with the Gaussian approximation at *steady state*. The results here show further that the approximation is excellent even in transient shear flows.

Figure 3 (a) shows that the GA-PG approximation is particularly useful in shear flows of moderate strength where fluctuations in the spring forces and HI are both important. The prediction of the GA-PG model is in remarkable agreement with simulations' results for the unsteady growth in the first normal-stress difference coefficient following the imposition of a moderate shear rate of  $\dot{\gamma}^* = 0.23$ . Similar quantitative agreement is obtained for the unsteady variation in  $\eta_p^*$  and  $R_e^{*2}$  at this shear rate. At lower shear rates, FE is not important, and the behaviour is the same as that obtained with Rouse chains, for which it was shown above that the Gaussian approximation does well in describing unsteady behaviour.

At high shear rates, where FE becomes the dominant

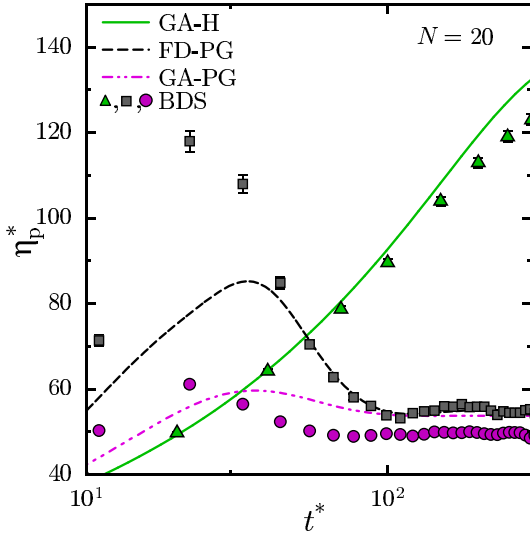


FIG. 4 Comparison of the predictions of the GA-H, FD-PG and GA-PG models for the growth of the shear viscosity with BDS results for Rouse chains with HI (green triangles), free-draining FENE chains (grey squares), and FENE chains with HI (magenta circles). The dimensionless shear rate is unity for Rouse chains and 0.91 for FENE chains.

effect, however, predictions of no single model are uniformly in agreement with the BDS results for all the properties examined, as illustrated in Fig. 3 (b). To understand the source of the deviations in the predictions of the GA-PG model, we compare in Fig. 4 predictions of the GA-H, FD-PG and GA-PG models at  $\dot{\gamma}^* \sim 1$ . The transient evolution of the viscosity in the GA-PG model can be broken into two phases: the early overshoot phase, and the later steady-state approach phase. At early times, we see that the GA-H model is in very good agreement with the BDS data (green triangles) for Rouse chains with HI. In the same period, the FD-PG predictions deviate quite strongly from the corresponding BDS data for free-draining FEBS chains (grey squares). The agreement of the composite GA-PG model with the BDS data for FEBS chains with HI (magenta circles) is thus seen to be intermediate in the overshoot phase. To understand the behaviour at steady state, we note that fluctuations in HI at high shear rates aid in the penetration of the solvent's velocity field into the deformed polymer coil, and the viscosity predicted is higher and closer to predictions with the corresponding free-draining model. This important aspect of HI's influence on the behaviour of dilute polymer solutions will be more clearly demonstrated shortly in predictions of steady state properties. From the overprediction of the viscosity by the GA-H model at large times in Fig. 4, we see that at high shear rates, the Gaussian approximation for HI overestimates the influence of fluctuations in HI. In Fig. 3 (b), we see that the CA-PG model's prediction is lower than the BDS results. The Gaussian approximation for HI thus pushes the viscosity prediction of the CA-PG past the BDS results.

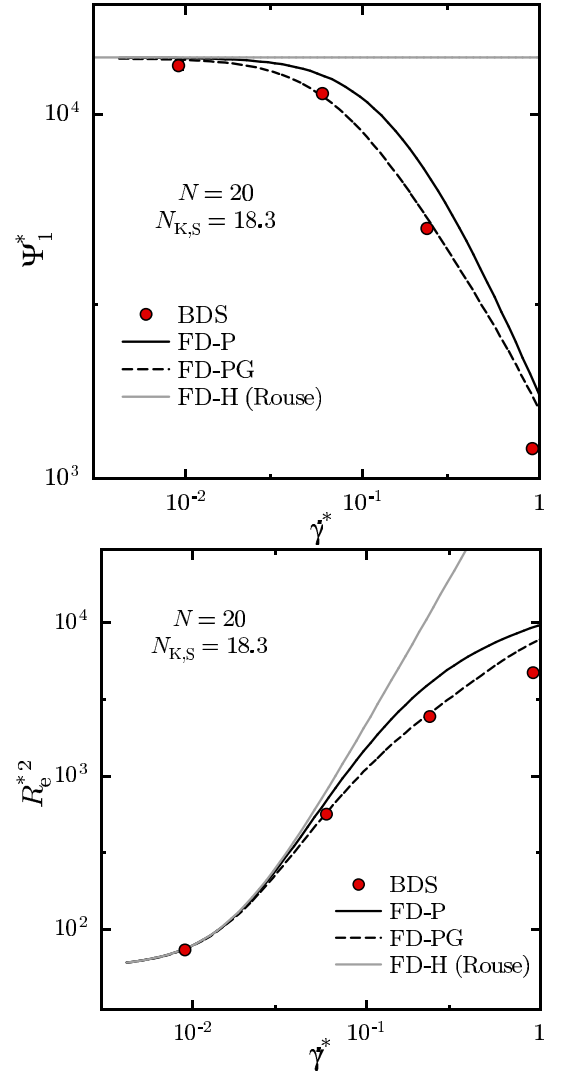


FIG. 5 Variation of (a) the steady-state first normal-stress difference coefficient, and (b) the steady-state mean-squared end-to-end distance, with shear rate, for free-draining FEBS chains.

## 2. Steady shear flow

The steady-state shear viscosity predicted by the FENE-P approximation has been observed earlier to be in quantitative agreement with the values obtained with BD simulations of small free-draining FENE chains<sup>37,38</sup>. For chains with  $N = 20$ , it is observed that the predictions of  $\eta_p^*$  obtained with the FENE-P and FENE-PG approximations are nearly identical. However, in Figs. 5 (a) and (b), it is seen that the FENE-PG approximation for the FENE force law does much better than the FENE-P approximation in its prediction of the steady-state  $\Psi_1^*$  and  $R_e^{*2}$ , respectively, at moderate shear rates. At  $\dot{\gamma}^* \approx 1$ , the predictions of  $R_e^{*2}$  and  $\Psi_1^*$  with FENE-PG springs also begin to deviate from BDS results significantly, but are closer to the exact results than the predictions obtained with FENE-P springs. From the

fact that the stresses and  $R_e^{*2}$  values predicted with simulations and the FD-PG model are lesser than the predictions of the FD-P model, we conclude that fluctuations in the spring forces lead to an increase in the effective stiffness of the chains.

As mentioned before, the predictions of the Gaussian approximation for Rouse chains in steady shear flows have been compared earlier with those of the Consistent- and Equilibrium-Averaging (Zimm) approximations, and with the results of exact BD simulations<sup>3,5</sup>. Figure 6 illustrates some of the key features of the predictions of the different approximations. As is well known, the net reduction in the average solvent velocity gradient within the polymeric coil<sup>22,49,50</sup> caused by HI results in smaller values of the shear viscosity at low to moderate shear rates, when compared to the free-draining Rouse model. The fact that the predictions of the Gaussian approximation and BD simulations are lower in Fig. 6 than those obtained with the Zimm and consistent-averaging approximations near equilibrium and at moderate shear rates, indicates that under these conditions, fluctuations in configurations at equilibrium result in a more effective screening of the velocity field within the coil. As the shear rate increases, the steady-state viscosity and the first normal stress difference coefficient first decrease in models with HI, other than the Zimm model. This shear-thinning, although not very strong, is a distinctive feature of configuration-dependent HI. The initial shear-thinning is observed to be more prominent with consistently-averaging than with the Gaussian approximation for HI. As the shear rate increases, the predictions of  $\eta_p^*$  and  $\Psi_1^*$  obtained with BD simulations, and the CA-H and GA-H models, reach a minimum with respect to the shear rate  $\dot{\gamma}^*$ . With a further increase in the shear rate, shear-thickening is observed in these models, wherein  $\eta_p^*$  and  $\Psi_1^*$  begin to increase towards the constant value predicted by the Rouse model in which HI is absent. The increase in  $\eta_p^*$  and  $\Psi_1^*$  towards the Rouse model's predictions is understood to be the consequence of the decreasing influence of HI as the average separation between the beads in the chains increases. Interestingly, in Fig. 6, the predictions of the GA-H model and the BD simulations' results lie above the curve predicted by the CA-H model beyond a threshold shear rate, and are closer to the free-draining Rouse model's prediction. This behaviour is contrary to that observed near equilibrium, and shows that the role played by fluctuations in HI reverses at higher shear rates, and in fact aid the penetration of the solvent velocity field into the polymer coil as the coil deforms and becomes highly anisotropic.

It is known that both the consistent-averaging and Gaussian approximations lead to shear rate dependent predictions for  $\Psi_2^*$ , which are opposite in sign for a large range of shear rates. This was first shown by Zylka<sup>5</sup>, thus demonstrating that fluctuations in HI lead to a change in the sign of  $\Psi_2^*$  at low to moderate shear rates for Rouse chains, inline with the results obtained here above for unsteady shear flow.

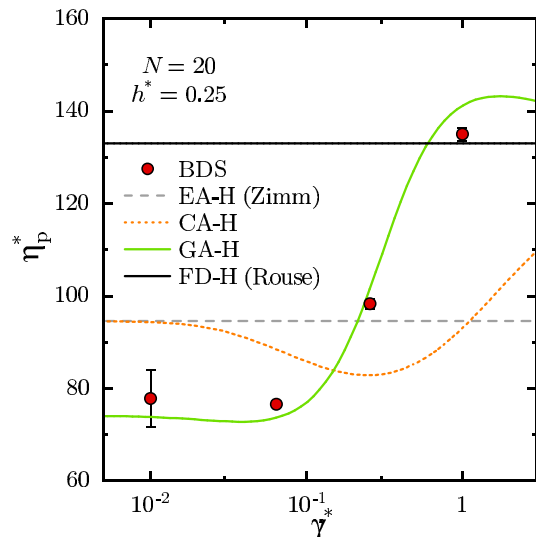


FIG. 6 The influence of HI on the variation of the steady-state polymer viscosity with dimensionless shear rate, for Rouse chains.

Figure 7 shows the results for the steady-state  $\Psi_1^*$  obtained with the different approximate models combining HI and FE. Predictions for the transient growth of  $\Psi_1^*$  at  $\dot{\gamma}^* = 0.23$  were presented earlier in Fig. 3 (a). The qualitative features of the predictions for the steady-state viscosity  $\eta_p^*$  are the same, although the shear-thinning-thickening behaviour is more pronounced in the case of  $\Psi_1^*$ . As before, the predictions of these models are compared with the results of BD simulations of FENE chains with fluctuating HI.

It is clear from Fig. 7 that among all the approximate models, only the predictions of the GA-PG model are close to the simulations' results across the whole range of shear rates examined. As one would expect, at low shear rates where the influence of FE is negligible, the observed behaviour is close to that observed for Rouse chains with HI, for which the Gaussian approximation for HI has been shown earlier to perform better than the Consistent-Averaging approximation. At moderate shear rates when FE begins to exert its influence, it is seen that the Gaussian approximation is not as accurate when used with FENE-P springs as it is with FENE-PG springs. This suggests that fluctuations in the spring forces also become important at moderately large shear rates. Interestingly, spring force fluctuations are however observed in Fig. 8 to have a negligible effect on the steady-state  $\Psi_2^*$ , and the predictions with the FENE-PG force expression are nearly the identical to those obtained with the FENE-P approximation.

As the shear rate increases further, the differences between the consistent-averaging and Gaussian approximations reduce for the same choice of the spring force law. However, it is observed<sup>27</sup> that at high shear rates, the predictions with models using the Gaussian Approximation for HI are closer to their free-draining counter-

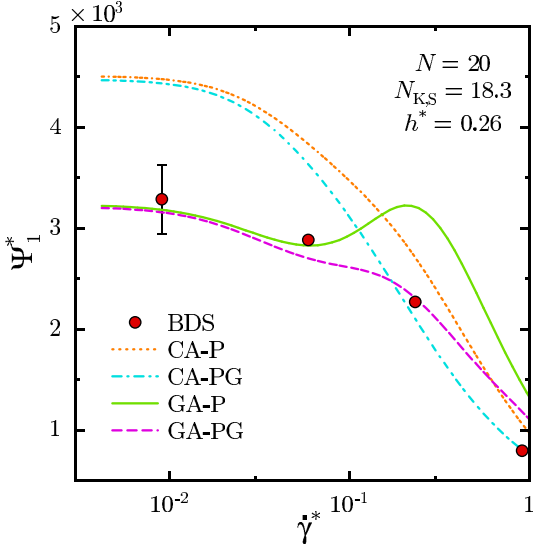


FIG. 7 Variation of the steady-state first normal-stress difference coefficient with shear rate, for FEBS chains with HI.

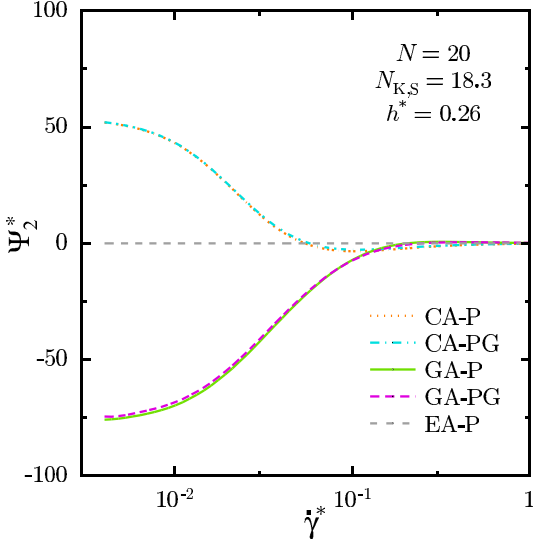


FIG. 8 Variation of the steady-state second normal-stress difference coefficient with shear rate, for FEBS chains with HI.

parts, than those using consistently-averaged HI. This behaviour once again points to the fact that fluctuations in HI aid in the penetration of the solvent's velocity gradient into the deformed polymer coil at higher shear rates.

Although at high shear rates Rouse chains with HI predict shear-thickening, FEBS models with HI predict shear-thinning. Kisbaugh and McHugh<sup>14</sup> showed using the diagonalized version of the CA-P model that complicated shear-thinning-thickening-thinning behaviour can occur as a result of the interplay between the emergence of FE and the fading of HI. Figure 9 shows the predictions of  $\eta_p^*$  obtained with the CA-PG and GA-PG models for chains with 25 springs, and  $N_{K,S} = 400$ . The behaviour in Fig. 9 suggests that the curve for the steady-state  $\eta_p^*$  predicted by a model combining the Gaussian

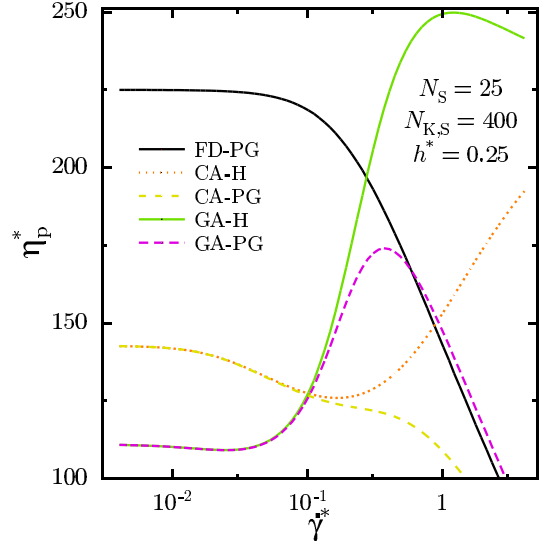


FIG. 9 Prediction of shear-thinning-thickening-thinning of the steady-state shear viscosity by models with HI, for  $N_K = 10^4$ .

Approximation for HI and the FENE-PG approximation for the nonlinear spring force is approximately bounded from above by the envelope formed by the Gaussian Approximation for Rouse chains at low to moderate shear rates, and by the terminal shear-thinning curve predicted by the free-draining model with the FENE-PG springs at high shear rates. The shear rate at which the  $\eta_p^*$ -versus- $\dot{\gamma}^*$  curves predicted by the two simpler models (*viz.* the GA-H and FD-PG models) intersect can be regarded as a critical shear rate  $\dot{\gamma}_c^*$ . At shear rates smaller than  $\dot{\gamma}_c^*$ , the overall behaviour of the polymer chains is dominated by HI, whereas FE is the dominant phenomenon when  $\dot{\gamma}^* > \dot{\gamma}_c^*$ .

## B. Extensional flow

### 1. Start-up and cessation of steady extensional flow

Models using Hookean springs predict unbounded extension in strong extensional flows. As a result of this unrealistic behaviour, the predictions of approximations for HI in Rouse chains have not been examined in strong and unsteady extensional flows. However, at any finite time following the imposition of the flow, the values of the stresses and other properties obtained with Rouse chains are still finite. Therefore, by comparing the predictions of the approximations and the results of BD simulations for Rouse chains one can study in isolation the influence of HI in strong extensional flows.

Figure 10 shows the growth of  $N_{1,p}^*$  upon the imposition of a steady extensional flow of  $\dot{\epsilon}^* = 0.04$  (which is greater than the critical strain rate for the coil-stretch transition  $\dot{\epsilon}_c^* = 0.012$  for  $N = 20$  and  $h^* = 0.25$ ). Also shown in Fig. 10 are the predictions for the relaxation of

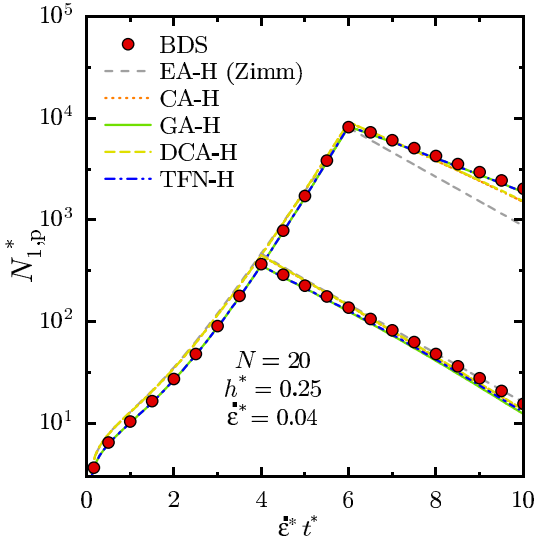


FIG. 10 Growth and decay of the polymer contribution to the first normal-stress difference for Rouse chains with HI, during start-up and following cessation of steady extensional flow, respectively.

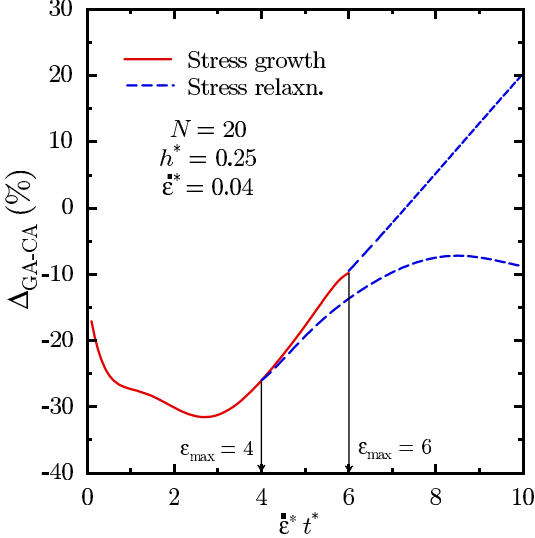


FIG. 11 Effect of fluctuations in HI on the growth and decay of the polymer contribution to the first normal-stress difference for Rouse chains with HI, during start-up and following cessation of steady extensional flow, respectively.

$N_{1,p}^*$  after the cessation of the extensional flow at different values of the Hencky strain.

The results in Fig. 10 show several fascinating features. Firstly, the predictions of all the approximate models, including the Zimm model with equilibrium-averaged HI appear to be in remarkably close agreement with the exact results of BDS in the stress growth phase. The Zimm model only begins to deviate noticeably from the rest of the data during stress relaxation after flow stoppage at high strains. Similar results are also obtained for  $R_e^{*2}$ . Although the differences between the different approximations appear to be small on the scale of the plot in

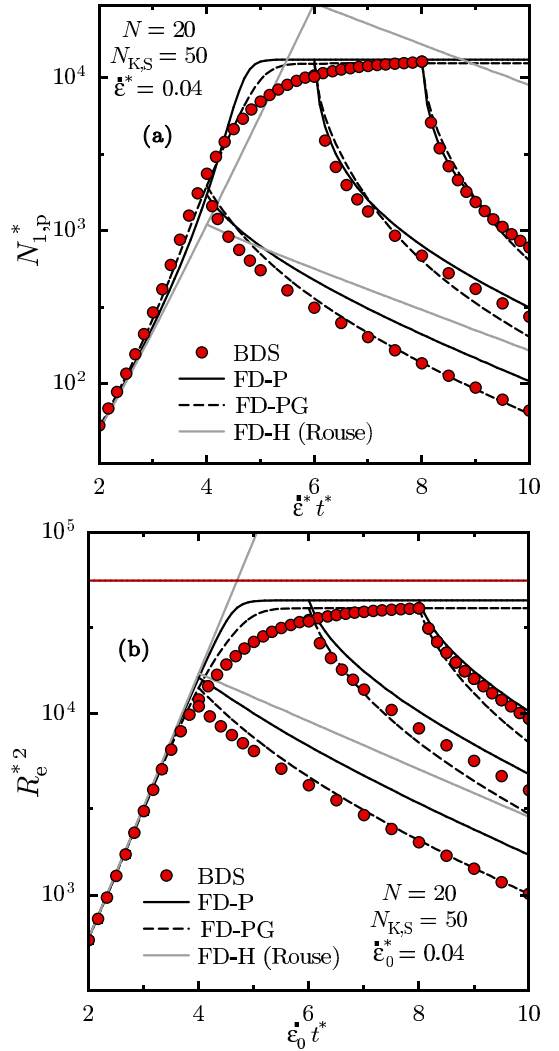


FIG. 12 Growth of (a) the polymer contribution to the first normal-stress difference, and (b) the mean-squared end-to-end distance of free-draining FEBS chains, during start-up, and their relaxation following cessation, of steady extensional flow. The horizontal red line in (b) indicates the maximum possible value of  $R_e^{*2} = 3N_{K,S}N_S^2$ .

Fig. 10, in Figure 11, the differences between the predictions of these approximations are examined more closely by plotting the relative difference between the predictions of  $N_{1,p}^*$  of the two approximations,

$$\Delta_{GA-CA} = \frac{N_{1,pGA}^* - N_{1,pCA}^*}{N_{1,pGA}^*}. \quad (78)$$

It is seen that fluctuations in HI can account for as much as 30% of the polymer stress in extensional flows.

Predictions of free-draining FEBS models employing the FENE-P and FENE-PG approximations are compared with exact results of the simulations for the growth and relaxation of  $N_{1,p}^*$  and  $R_e^{*2}$  in Figs. 12 (a) and (b), respectively. Also shown for comparison are the predictions of the simple Rouse model. The strain-rate for

which the data are shown in Fig. 12 is larger than the critical strain rate  $\dot{\epsilon}_c^* = \sin^2(\pi/2N) = 6.2 \times 10^{-3}$  for free-draining chains with  $N = 20$ . At this relatively high strain rate, the Rouse model predicts an exponential increase in both  $N_{1,p}^*$  and  $R_e^{*2}$  during extension. At small values of the Hencky strain during start-up of the extensional flow at this strain rate, all the data for the different models are essentially identical, since the springs are not stretched sufficiently for the spring-force nonlinearities to have any significant effects. The influence of FE is first discerned in the growth of the stress when the curves for the FEBS chains separate from the prediction of the Rouse model. At higher strains, the deviations between the approximations and the exact results for  $N_{1,p}^*$  become more marked and reach a maximum when the approximate results level off sharply towards their eventual steady-states. The approach of the BD simulations' data to steady-state is more gradual. In the stress growth phase, the predictions of the FENE-PG approximation are closer to the exact results, than those obtained with the FENE-P approximation.

The relaxation behaviour of free-draining FEBS chains following the cessation of extensional flow has been previously studied<sup>23,51</sup>. While Doyle et al. compared the predictions of the FENE-PM approximation with BD simulations of FENE dumbbells and also bead-rod chains, Wiest examined some interesting qualitative features in the stress-relaxation phase using the FENE-P model.

The FENE-PG approximation is seen to lead to more accurate description of both the stress and extension in the relaxation phase when the strain at flow stoppage is not much larger than the strain at which FE begins to exert its influence, whereas the FENE-P approximation leads to an overprediction of both properties. When the Hencky strain at flow stoppage is larger, the FENE-PG force law is seen to be in fact less trustworthy. This loss in accuracy of the FENE-PG model when chains are highly stretched is consistent with the behaviour observed earlier in steady and unsteady shear flow.

The predictions of approximate models with both non-linear phenomena incorporated, for the unsteady growth and relaxation of  $N_{1,p}^*$  and  $R_e^{*2}$  following start-up and cessation of an extensional flow are shown in Figs. 13 (a) and (b). The initial behaviour ( $\epsilon \leq 4$ ) in the stress-growth phase is close to that observed for Rouse chains with HI since the influence of FE is weak at these strains. The differences between the various approximations grow larger at intermediate strains during extension. At these strains and above, the curves predicted by the combined models are qualitatively similar to the predictions obtained with the approximations for free-draining FEBS chains. In particular, the nature of deviations between the BD simulations' results and the approximations' predictions appear to be decided largely by the approximation used for the FENE nonlinearity. At higher strains, as chain become highly stretched, incorporating fluctuations in HI through the Gaussian Approximation make the curves predicted by the combined models lie closer

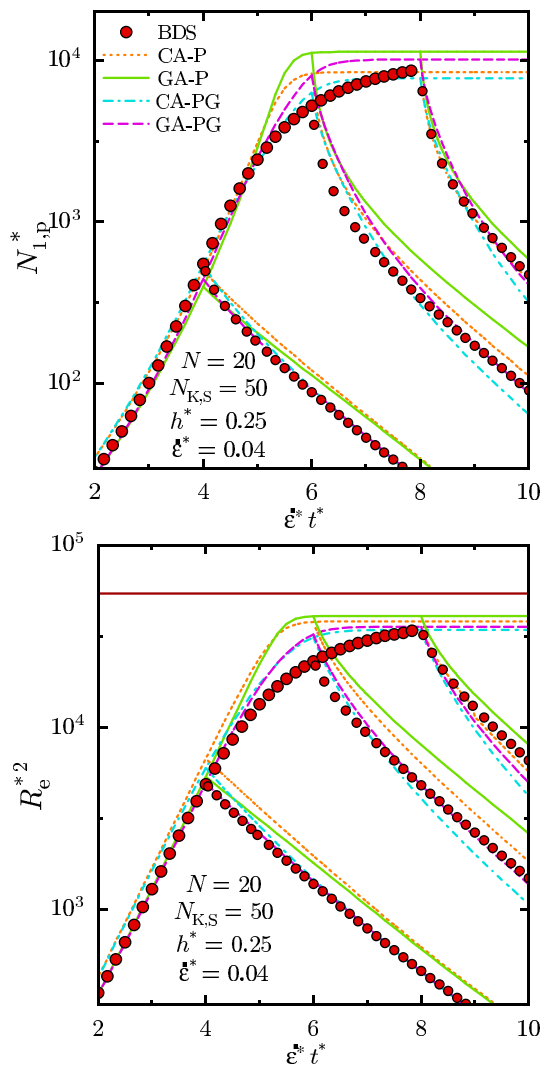


FIG. 13 Growth and decay of the polymer contribution to (a) the dimensionless first normal-stress difference, and (b) the mean-squared end-to-end distance, for FEBS chains with HI, during start-up and following cessation, of steady extensional flow. The horizontal red line indicates the maximum possible value of  $R_e^{*2} = 3 N_{K,S} N_S^2$ .

to those obtained with the corresponding free-draining model<sup>27</sup>. Predictions of the relaxation behaviour are observed to be better with the FENE-PG force law when the strain at flow stoppage is low. The largest deviations in the approximations' predictions of the relaxation behaviour occur when flow is stopped at a strain in the “knee” region just prior to steady-state. On the whole, the GA-PG model appears to be quite accurate in its description of the normal stresses and chain deformation in unsteady extensional flows.

The prediction of stress-conformation hysteresis is another test of the accuracy of closure approximations. Stress-conformation hysteresis in dilute polymer solutions has been studied in experiments<sup>52,53</sup> and theoretically<sup>23,39,40,51,54</sup>. In extensional flow experi-

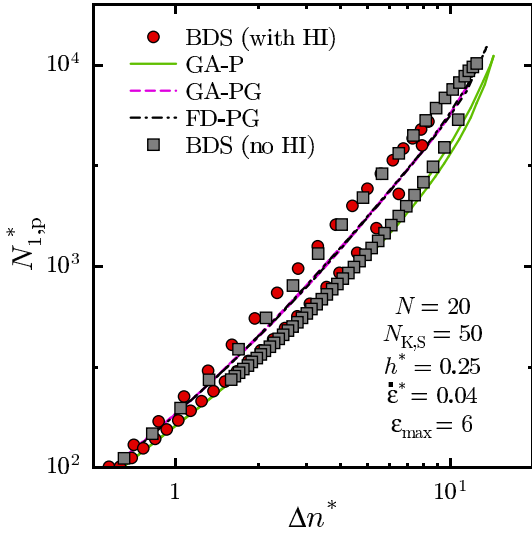


FIG. 14 Stress-conformation hysteresis for FEBS chains with and without HI.

ments, it is observed that when the normal stress is plotted against the birefringence of the solution, the curves described by the data points during the stress-growth and stress-relaxation phases are very different. In particular, at any fixed value of the birefringence, the stress during extension is larger than that measured during relaxation. Conversely, at a fixed stress, the birefringence during relaxation is larger.

Figure 14 compares the  $N_{1,p}^*$ -versus- $\Delta n^*$  behaviour predicted by BD simulations and the various approximations. It is immediately clear that closure approximations fail to reproduce the size of the hysteresis loops observed in the simulations. Models using the FENE-P springs predict larger birefringence than the exact simulations at any level of the stress. When fluctuations are accounted for in the spring forces through the FENE-PG force law, the size of the hysteresis loop becomes even smaller. Nevertheless, the curves predicted with FENE-PG springs now lie within the loops predicted by the BD simulations.

Remarkably, HI appears to have almost no influence on stress-configuration hysteresis. Although the maximum values of the stress and  $\Delta n^*$  are larger when free-draining models are used, the simulations' and approximations' predictions with and without HI show significant overlap. Similar behaviour is also observed on a plot of  $N_{1,p}^*$ -versus- $R_e^*$ <sup>227</sup>. The reason behind this insensitivity of stress-conformational hysteretic behaviour to HI is not understood.

## 2. Steady extensional flow

Figure 15 compares the predictions of the steady-state polymer extensional viscosity by different approximations with the simulations' results obtained for FEBS chains with and without HI. The BDS results were ob-

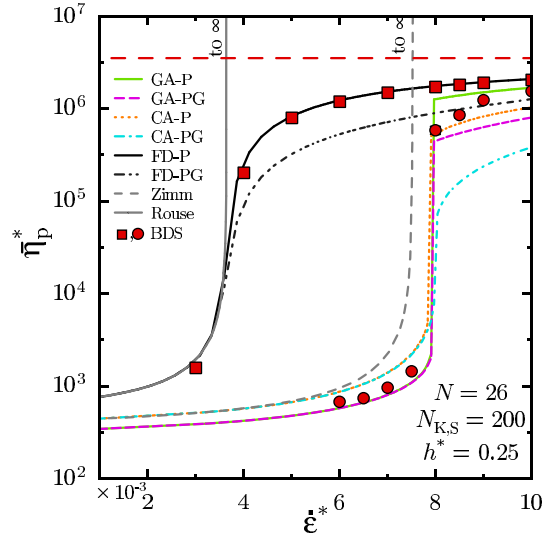


FIG. 15 Variation of the steady-state polymer extensional viscosity with extension-rate, for FEBS chains with HI and without HI. The red square and circle symbols represent results obtained with BDS of FEBS chains with and without HI respectively. The horizontal dashed red line is the dimensionless extensional viscosity of fully-stretched free-draining chains calculated using Eq. 79, and marks the upper limit of the extensional viscosity for FEBS chains with parameter values shown.

tained using step changes in the extension rates and integrating until a steady value is obtained for  $\eta_p^*$  at each extension rate. The most important characteristic of the curves for the steady-state extensional viscosity is the occurrence of a sudden rapid increase in its value within a narrow range of strain rates around a critical elongation rate  $\dot{\epsilon}_c^*$ . As is well known, the value of  $\dot{\epsilon}_c^*$  can be calculated analytically in the Rouse model to be  $\dot{\epsilon}_c^* = 0.5/\tau_1^{*R} = \sin^2(\pi/2N)$ <sup>16</sup> at which the steady-state  $\bar{\eta}_p^*$  predicted by the Rouse model diverges. A similar divergence is predicted with the Zimm model at  $\dot{\epsilon}_c^* = 0.5/\tau_1^{*Z}$ . Here,  $\tau_1^{*R}$  and  $\tau_1^{*Z}$  are the largest time constants in the Rouse and Zimm models. For FEBS chains with or without HI,  $\bar{\eta}_p^*$  remains bounded by the limit for fully-stretched free-draining chains completely aligned in the direction of extension<sup>55</sup>,

$$\bar{\eta}_p^* = N_{K,S} N_S (N_S + 1) (N_S + 2). \quad (79)$$

As observed earlier in shear flows, the steady-state  $\bar{\eta}_p^*$ -versus- $\dot{\epsilon}^*$  curves predicted by models with FEBS chains are indistinguishable from those obtained with Rouse chains until FE becomes important. Predictions with the FD-P approximation in the super-critical regime ( $\dot{\epsilon}^* > \dot{\epsilon}_c^*$ ) are in remarkable agreement with the BDS results, whereas the FD-PG approximation significantly underpredicts the exact results. The accuracy of the FD-P approximation in its prediction of the steady-state extensional viscosity is well known<sup>38</sup>. This behaviour however is in contrast with that observed in steady shear

flows (Fig. 5), where the FD-PG approximation’s prediction are closer to the simulations’ results even at high shear rates.

As mentioned earlier, Liens *et al.*<sup>40</sup> and Wiest<sup>34</sup> have argued that the accuracy of the FENE-P approximation at high extension rates stems from the fact that the exact distribution of spring lengths is very narrow and close to being a  $\delta$ -function centered at some value  $\bar{Q}$  lesser than  $Q_0$ . Under such conditions, the FENE nonlinearity  $\xi$  is well approximated by the FENE-P function  $\bar{\xi}$ . When  $\bar{Q}$  is not very close to  $Q_0$ , it is clear that the additional term in the FENE-PG function  $\mathbf{L}$  in Eq. (34) leads to inaccuracies.

We recall that higher order terms in the series expansion in Eq. (28) have been dropped in obtaining  $\mathbf{L}$  in Eq. (34). Since every term [Eq. (30)] in the series in Eq. (28) is positive, it is evident that *after* applying the Peterlin approximation to every term in the series, the full summation (if convergent) will lead to an even greater overestimation of the influence of spring-force fluctuations when the true spring length distribution is narrow. Since the series expansion in Eq. (28) itself has been derived under the assumption of a Gaussian distribution, it appears that the extension of the Gaussian approximation to the FENE springs may not be appropriate in situations where the spring length distribution is narrow, but  $\bar{Q}$  is not close to  $Q_0$ . The better agreement of predictions with FENE-PG springs with BDS data observed earlier in shear flows not only indicates that spring length fluctuations are larger in shear flows, but also shows that the Gaussian approximation captures the influence of these fluctuations more accurately. As the strain-rate increases and  $\bar{Q}$  approaches  $Q_0$ , it was shown in section III.A that the additional contribution in the FENE-PG spring force becomes negligible in comparison with  $\bar{\xi}$ , and the differences between the predictions of the two approximations become smaller.

For chains with HI, the superiority of the Gaussian approximation is clearly evident in Fig. 15, in the sub-critical regime. At strain-rates greater than  $\dot{\epsilon}_c^*$ , it is the GA-P model that performs best (also see Fig. 16 below). This is somewhat surprising, since one might expect from the better performance of the FD-P model for free-draining chains observed earlier, that fluctuations are small when chains are stretched out in the super-critical regime. Therefore, if the influence of both spring-force and HI fluctuations are unimportant, the predictions of the CA-P model should be close to the BDS data. Instead, however, the GA-P model does much better than the CA-P model in Fig. 15. One plausible explanation for this observation could be that although fluctuations in spring lengths may be small and the FENE-P approximation for the spring force is accurate, the distribution of overall chain configurations may not be as sharply peaked at strain rates above  $\dot{\epsilon}_c^*$ . The resultant fluctuations in HI may therefore may still play an important role. The GA-PG model underpredicts the BDS results for the extensional viscosity when  $\dot{\epsilon}^* > \dot{\epsilon}_c^*$ , and this is seen to be

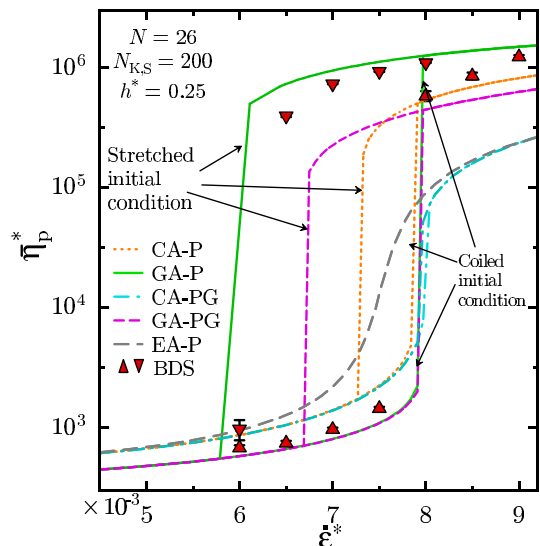


FIG. 16 Prediction of coil-stretch hysteresis in the steady-state extensional viscosity by closure approximations for FEBS chains with HI. The upright and inverted triangle symbols represent BDS data obtained by successively stepping up, and stepping down, the extension rate, respectively.

the result of the inaccuracy of the FENE-PG spring force at high extensions.

It is observed that the approximations for FEBS chains with HI can predict multiple steady-state values for the extensional viscosity for a range of values of the extension rate  $\dot{\epsilon}^*$  [Fig. 16]. The variation of the steady-state extensional viscosity with extension-rate predicted by the approximations in Fig. 16 was obtained as follows. Starting with the equilibrium second moments ( $\sigma_{ij,eq}^* = \delta_{ij}\delta$ ) as the initial guess, the set of coupled, nonlinear equations for the steady-state second moments were first iteratively solved at a small value ( $\ll \dot{\epsilon}_c^*$ ) of the extension rate. After calculating the extensional viscosity with the converged solution for the equilibrium second moments, this solution is used as the guess for obtaining the solution numerically at a slightly larger value of  $\dot{\epsilon}^*$ . This process is continued until  $\dot{\epsilon}^*$  is well beyond the value of  $\dot{\epsilon}_c^*$  for the coil-to-stretch transition. The  $\bar{\eta}_p^*$ -versus- $\dot{\epsilon}^*$  curve obtained thus is indicated as having been obtained with a “coiled initial condition” in Fig. 16. The process is then reversed by successively lowering the extension-rate. In Fig. 16, it is seen that with the notable exception of the EA-P model, the predicted  $\bar{\eta}_p^*$ -versus- $\dot{\epsilon}^*$  curve follows a different route as  $\dot{\epsilon}^*$  is decreased for all the other approximations for chains with HI. Since this steady-state solution branch is obtained starting from a highly “stretched initial condition”, it is indicated as such in Fig. 16. A similar procedure described earlier by Schroeder *et al.*<sup>56</sup> was used to obtain the BDS data.

The existence of such “coil-stretch hysteresis” was first proposed in a landmark study by De Gennes<sup>57</sup>, who used a variable friction coefficient in a simple dumbbell model to model the effect of the deformation of the polymer

coil on its hydrodynamics. A further closure approximation equivalent to the consistent-averaging treatment was used to obtain a solvable dumbbell model that predicted coil-stretch hysteresis in a uniaxial extensional flow. To the best of our knowledge, Fig. 16 is the first demonstration that closure approximations for FEBS chain models with HI can predict coil-stretch hysteresis.

It is interesting to note that the size of the window of strain rates where multiple steady-states are obtained, depends strongly on the approximation used. The window size appears to depend on the difference between the extensional viscosities in the coiled state (the lower branch of the hysteresis curve) and the stretched state (the upper branch of the hysteresis curve). Fluctuations in HI lead to a widening of the window because these fluctuations decrease  $\bar{\eta}_p^*$  in the coiled state, but increase  $\bar{\eta}_p^*$  when the chains are highly stretched. As before, the BDS data are quite close to the predictions of the GA-P model. Significantly, multiple steady-states are never obtained with the EA-P model, and in the free-draining models. As pointed out by De Gennes, coil-stretch hysteresis occurs principally because of the modification of the mobility matrix due to the deformation of the polymer coil. With equilibrium averaged HI (and in all free-draining models), the mobility matrix is deformation-independent, and hence no coil-stretch hysteresis is observed.

As mentioned above, De Gennes first obtained such multiple steady-states using a mean-field closure approximation in a simple dumbbell model with a variable configuration-dependent drag coefficient. Later, Fan *et al.*<sup>58</sup> obtained the solution to the Fokker-Planck equation for the dumbbell model numerically without using any closure approximations, and found that the resulting steady-state expectations are single-valued functions of the extension rate. They argued that De Gennes' prediction of a coil-stretch hysteresis must therefore be an artifact of the mean-field approximations used in his model. More recently, Schroeder *et al.*<sup>59</sup> showed that the exact steady-state configurational distribution in the variable drag dumbbell model is bi-modal, and that a large (effective) free energy barrier between the coiled and stretched states leads to ergodicity-breaking. In contrast, however, the use of closure approximations leads to two distinct uni-modal Gaussian solutions to the modified Fokker-Planck equations.

The BDS results obtained by Schroeder *et al.*<sup>59</sup>, and those in Fig. 16 suggest that the exact distribution of the steady-state extensional stress in FEBS chains with HI is also bi-modal. The linearity of the Fokker-Planck equation [Eq. (1)] in the configurational probability distribution function further guarantees that its exact solution is unique. The introduction of any mean-field approximation however leads to a modified Fokker-Planck equation that is nonlinear in the probability distribution function, since the coefficients in the modified Fokker-Planck equation are functionals of the distribution function. While the solution of this modified equation may be a uni-modal

Gaussian distribution, the nonlinearity in the distribution function means that the solution may no longer be unique. Thus, the exchange of the nonlinearities due to FENE and HI for a nonlinearity in the distribution function destroys the multi-modal nature of the original solution, but allows the modified Fokker-Planck equation to have multiple solutions.

In spite of the fundamentally different probability distributions, the results presented in Fig. 16 above indicate that the multiple steady-states obtained with the approximations can closely follow the long-lived kinetically trapped states in the original model. Therefore, closure approximations for FEBS chains with HI may prove to be useful in a detailed exploration of hysteretic phenomena caused by ergodicity-breaking in dilute polymer solutions.

We next briefly discuss the accuracy of the diagonalization approximations in shear and extensional flows.

### C. Two-fold Normal Approximation

Figure 17 compares the predictions at high shear and extension rates obtained with the diagonalized DGA-H, DFD-P and TFN-P approximations and their respective un-diagonalized versions, namely, the GA-H, FD-P and GA-P approximations. The effect of making the diagonalization assumption is examined here by calculating the relative deviation between the predictions of a property  $\pi$  obtained with an approximation "A" and its diagonalized version "DA":

$$\Delta_{D,\pi} \equiv \frac{\pi_{DA} - \pi_A}{\pi_A}. \quad (80)$$

Figures 17 (a) and (b) demonstrate that the relative deviation between the predictions of GA-P model and its diagonalized version in shear flow, the TFN-P model, can be quite significant. In contrast, the diagonalization assumption is much more accurate for approximations for Rouse chains with HI (the GA-H and TFN-H models), for which the largest relative deviation does not exceed 10% in Fig. 17 (a) and (b). On the other hand, the overall time variation of the deviation between the TFN-P and GA-P models is qualitatively similar to that observed between the diagonalized FD-P (DFD-P) model and the FD-P model, but is smaller in magnitude. The magnitude of the deviations depend on the property considered. In shear flows, the deviations in the predictions for  $\eta_p^*$  are smaller. In both shear and extensional flows, the deviations are larger in the predictions of  $R_e^{*2}$  than in the stresses.

The results above indicate that for Rouse chains, or for FEBS chains at low strains and/ or strain-rate, when FE is unimportant, the inclusion of HI diminishes the influence of the off-diagonal components of the normal-mode covariances on the overall behaviour predicted by the models, and the diagonalization approximations are

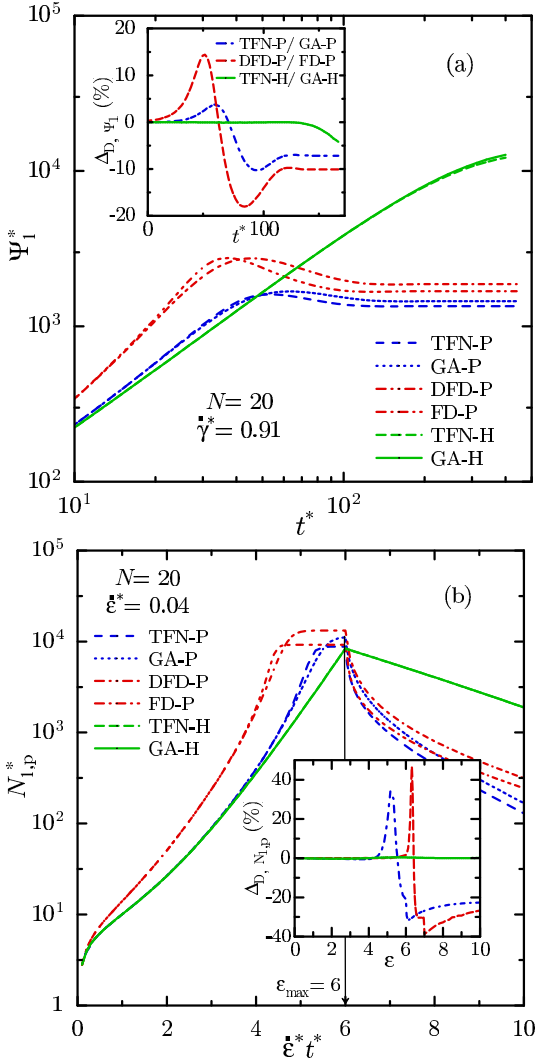


FIG. 17 Predictions of the diagonalization approximations for (a) the growth of the first normal-stress difference coefficient after imposition of a steady shear rate, and (b) the growth and relaxation of the polymer contribution to the dimensionless first normal-stress difference, during start-up and following cessation, of steady extensional flow. In (a),  $N_{k,s} = 18.3$  for models with FENE-P springs, and  $h^* = 0.25$  for models with HI. In (b),  $N_{k,s} = 50$  for models with FENE-P springs, and  $h^* = 0.25$  for models with HI. The insets plot the relative deviations of the predictions of the diagonalized and un-diagonalized approximations, calculated using Eq. (80).

quite accurate. The diagonalization assumption begins to break down when FE begins to exert its influence.

In spite of the deterioration in the quality of the diagonalization approximations when FE is important, the massive reduction in CPU-time usage (Table II) achieved with these approximations make them an ideal tool for rapid preliminary exploration of vast regions of parameter space. In fact, Eq. (60) coupled with the equation for the polymer stress in Eq. (39), constitute a new constitutive model for the polymer stress in dilute polymer solu-

TABLE II Sample comparison of CPU-time requirements for BD simulations, un-diagonalized and diagonalized approximations. The value reported for BD simulations is for  $10^4$  trajectories. For  $N = 160$ , the reported value has been calculated from the CPU-time required for 200 trajectories. The CPU-times reported for the CA-P and GA-P approximations for  $N = 160$  have been projected from the CPU-time-versus- $N$  scaling observed for  $20 \leq N \leq 100$ . All calculations were performed on 2.66 GHz, Pentium 4 (Dell Precision 250) processors.

N	CPU-time in hrs.			
	BDS	CA-P	GA-P	TFN-P
60	220	10	51	0.9
160	10012	2073	3131	32

tions. This constitutive model reproduces all the key features characteristic of these solutions with reasonable accuracy, including coil-stretch hysteresis (not shown here), and thus represents a significant improvement over constitutive equations such as the Oldroyd-B or FENE-P dumbbell equations typically used in the simulation of complex flows of dilute polymer solutions.

## VII. SUMMARY AND CONCLUSIONS

The Gaussian Approximation was originally suggested for Hookean dumbbells and Rouse chains with HI by Öttinger<sup>3</sup> and Wedgewood<sup>4</sup>, and has been shown to improve predictions by approximately accounting for the influence of fluctuations in HI. In this work, we use the same idea in the context of a free-draining bead-FENE spring model to first obtain a new approximation for tackling the closure problem posed by the FENE nonlinearity. We show that the resulting equations in the approximate model can be interpreted in terms of a mean-field spring potential, and that this “FENE-PG” spring potential improves upon the well known FENE-P approximation in situations where spring force fluctuations are important. Furthermore, the use of additional diagonalization-of-normal-modes assumptions for simplifying the model equations lead to considerable savings in computation time, without significant loss in accuracy.

The direct application of the Gaussian Approximation for bead-spring models simultaneously incorporating the effects of both FE and HI leads to an undesirable dependence of the predictions of equilibrium static properties on the hydrodynamic interaction parameter,  $h^*$ . Instead, we use a two-step procedure to marry the FENE-PG mean-field spring potential with the Gaussian Approximation for HI to arrive at a closed set of equations for the second-moments, which is consistent with the equilibrium Boltzmann probability distribution. This approximate model accounts for the influence of fluctuations in both HI and the spring forces.

The method of combining the Gaussian approximation for HI with the FENE-PG approximation for HI suggested in this study is found to lead to predictions that compare well with the results of exact BD simulations for properties in steady and unsteady shear flows. The better agreement of the predictions of this approximate model—dubbed here as the “GA-PG” model—than those obtained with the FENE-P and/or Consistent-Averaging approximations emphasizes the importance of fluctuations in HI, and also highlights the role spring force fluctuations play at moderate and high shear rates. In extensional flows, the GA-P model combining the Gaussian approximation for HI with FENE-P springs is found to perform better when chains are highly stretched, perhaps indicating that under such conditions, fluctuations in HI may still be important, even though local fluctuations in spring lengths are small.

The predictions obtained with the Gaussian approximation for HI in steady and unsteady shear and extensional flows confirms previous observations on the role of fluctuations in HI on macroscopic behaviour. When chains are close to their equilibrium isotropic states, fluctuations in HI enhance the screening of the solvent velocity gradient caused by HI. The role of fluctuations in HI reverses in situations where polymer chains experience significant stretching, and aid the penetration of the velocity field into the stretched polymer coil. Consequently, the solvent is able to engage a firmer “grip” on the chains and this tends to deform an already anisotropic chain further. Fluctuations in the FENE spring force are found to increase the chains’ resistance to stretching.

When the stress predicted in BD simulations of FEBS chains during the start-up and following the cessation of a strong extensional flow is plotted against predictions of the mean-squared end-to-end distance of the chains, or against the intrinsic birefringence, large hysteresis loops were observed. The hysteresis loops predicted with closure approximations were much smaller than those predicted with the simulations. Surprisingly, HI was found to have a negligible influence on the phenomenon of stress-conformational hysteresis observed in extensional flows.

Closure approximations for FEBS chains with HI predict coil-stretch hysteresis. In particular, predictions of hysteresis in the extensional viscosity by the GA-P model are in excellent agreement with the exact results obtained with BD simulations. It is observed that fluctuations in HI enhance the hysteretic effect, increasing the width of the coil-stretch hysteresis window on a plot of the steady-state extensional viscosity versus the strain-rate.

#### APPENDIX A: Tensors associated with hydrodynamic interactions

The tensor  $\bar{\mathbf{A}}_{ij}$  in Eq. (48), which describes contributions arising from averaging the Oseen-Burgers tensor with the non-equilibrium distribution function, is given

by the expression,

$$\bar{\mathbf{A}}_{ij} \equiv \langle \tilde{\mathbf{A}}_{ij} \rangle = A_{ij} \boldsymbol{\delta} + \sqrt{2} h^* [\mathbf{H}_{ij} + \mathbf{H}_{i+1, j+1} - \mathbf{H}_{i+1, j} - \mathbf{H}_{i, j+1}], \quad (\text{A1})$$

while the tensors  $\Delta_{ij}$  and  $\Delta_{ij}^T$ , which represent contributions due to fluctuations in HI, are given by,

$$\Delta_{ij} \equiv \sum_{r,s=1}^{N_s} \Gamma_{rj}^{is} : (\boldsymbol{\sigma}_{sr}^* \cdot \mathbf{L}_r),$$

and,

$$\Delta_{ij}^T = \sum_{r,s=1}^{N_s} (\mathbf{L}_r \cdot \boldsymbol{\sigma}_{rs}^*) : \Gamma_{jr}^{si}, \quad (\text{A2})$$

with,

$$\Gamma_{rq}^{ps} \equiv \frac{3\sqrt{2}h^*}{4} [\Delta \Theta_{rq}^{ps} \mathbf{K}_{rq} + \Delta \Theta_{r+1, q+1}^{ps} \mathbf{K}_{r+1, q+1} - \Delta \Theta_{r+1, q}^{ps} \mathbf{K}_{r+1, q} - \Delta \Theta_{r, q+1}^{ps} \mathbf{K}_{r, q+1}]. \quad (\text{A3})$$

The second-rank tensorial function  $\mathbf{H}_{\nu\mu} = \mathbf{H}(\mathbf{S}_{\mu\nu}^*)$  is related to the average of the HI tensor through,

$$\langle \zeta \boldsymbol{\Omega}_{\nu\mu} \rangle = \sqrt{2} h^* \mathbf{H}(\mathbf{S}_{\mu\nu}^*), \quad (\text{A4})$$

whereas the fourth-rank tensorial function  $\mathbf{K}_{\mu\nu} = \mathbf{K}(\mathbf{S}_{\mu\nu}^*)$  is related to the HI tensors through,

$$\left\langle \frac{\partial(\zeta \boldsymbol{\Omega}_{\nu\mu})}{\partial \mathbf{r}_{\mu\nu}} \mathbf{r}_{\mu\nu} \right\rangle = \frac{3\sqrt{2}h^*}{4} \mathbf{K}(\mathbf{S}_{\mu\nu}^*) \cdot \mathbf{S}_{\mu\nu}^*. \quad (\text{A5})$$

In the equations above,

$$\mathbf{S}_{\mu\nu}^* = \langle \mathbf{r}_{\mu\nu}^* \mathbf{r}_{\mu\nu}^* \rangle = \sum_{i,j=1}^{N_s} \Delta \Theta_{\mu\nu}^{ij} \boldsymbol{\sigma}_{ij}^*. \quad (\text{A6})$$

Here,

$$\Delta \Theta_{\mu\nu}^i = \begin{cases} 1, & \text{if } \mu \leq i < \nu, \\ -1, & \text{if } \nu \leq i < \mu, \\ 0, & \text{otherwise,} \end{cases} \quad (\text{A7})$$

is the one-dimensional “box” function. This function can be succinctly expressed in terms of the Heaviside step function,

$$\Theta(m, n) = \begin{cases} 1, & \text{if } n \geq m \\ 0 & \text{otherwise,} \end{cases} \quad (\text{A8})$$

as  $\Delta \Theta_{\mu\nu}^i = \Theta(\mu, i) - \Theta(\nu, i) = -\Delta \Theta_{\nu\mu}^i$ . Further, the dyad

$$\mathbf{r}_{\mu\nu} \mathbf{r}_{\mu\nu} = \sum_{i,j=\min(\nu,\mu)}^{\max(\nu,\mu)-1} \mathbf{Q}_i \mathbf{Q}_i = \sum_{i,j=1}^{N_s} \Delta \Theta_{\mu\nu}^{ij} \mathbf{Q}_i \mathbf{Q}_j, \quad (\text{A9})$$

where the two-dimensional box function,

$$\Delta\Theta_{\mu\nu}^{ij} = \Delta\Theta_{\mu\nu}^i \Delta\Theta_{\mu\nu}^j. \quad (\text{A10})$$

This function is symmetric with respect to an exchange of the indices  $\mu$  and  $\nu$ , and/or  $i$  and  $j$ .

When the Oseen-Burgers form of the HI tensor is used, it can be shown that<sup>2,60</sup>

$$\mathbf{H}_{\nu\mu} = \frac{3}{2(2\pi)^{3/2}} \int \frac{1}{k^2} \left( \delta - \frac{\mathbf{k}\mathbf{k}}{k^2} \right) \exp\left(-\frac{1}{2} \mathbf{k}\mathbf{k} : \mathbf{S}_{\mu\nu}^* \right) d\mathbf{k}, \quad (\text{A11})$$

and

$$\mathbf{K}_{\nu\mu} = \frac{-2}{(2\pi)^{3/2}} \int \frac{1}{k^2} \mathbf{k} \left( \delta - \frac{\mathbf{k}\mathbf{k}}{k^2} \right) \mathbf{k} \exp\left(-\frac{1}{2} \mathbf{k}\mathbf{k} : \mathbf{S}_{\mu\nu}^* \right) d\mathbf{k}, \quad (\text{A12})$$

Thus, the functions  $\mathbf{H}_{\nu\mu}$  and  $\mathbf{K}_{\nu\mu}$ , and therefore  $\bar{\mathbf{A}}_{ij}$  and  $\Delta_{ij}$  are completely expressible in terms of the second moments of the Gaussian distribution.

The inner product of  $\mathbf{K}$  with a second-rank tensor  $\mathbf{a}$  is defined in component form as

$$(\mathbf{K} : \mathbf{a})_{\alpha\beta} = \sum_{\gamma,\delta=1}^3 K_{\alpha\beta\gamma\delta} a_{\delta\gamma}, \quad (\text{A13})$$

and,

$$(\mathbf{a} : \mathbf{K})_{\alpha\beta} = \sum_{\gamma,\delta=1}^3 a_{\delta\gamma} K_{\gamma\delta\alpha\beta} \text{ for } \alpha, \beta = 1, 2, 3. \quad (\text{A14})$$

Further, since the inner product

$$\frac{1}{k^2} \left( \delta - \frac{\mathbf{k}\mathbf{k}}{k^2} \right) \mathbf{k} : \delta = \mathbf{0},$$

for all  $\mathbf{k}$ , we have

$$\mathbf{K} : \delta = \mathbf{0}. \quad (\text{A15})$$

A direct consequence of this result is that the  $\Delta$  tensors defined through Eqs. (A2) and (A3), vanish under isotropic equilibrium conditions.

## References

- [1] B. H. Zimm. Dynamics of polymer molecules in dilute solution: Viscoelasticity, flow birefringence and dielectric loss. *J. Chem. Phys.*, 24(2):269–278, 1956. URL <http://dx.doi.org/10.1063/1.1742462>.
- [2] H. C. Öttinger. Generalized Zimm model for dilute polymer solutions under theta conditions. *J. Chem. Phys.*, 86(6):3731–3749, 1987. URL <http://dx.doi.org/10.1063/1.451975>.
- [3] H. C. Öttinger. Gaussian approximation for Rouse chains with hydrodynamic interaction. *J. Chem. Phys.*, 90(1):463–473, 1989. URL <http://dx.doi.org/10.1063/1.456496>.
- [4] L. E. Wedgewood. A Gaussian closure of the second-moment equation for a Hookean dumbbell with hydrodynamic interaction. *J. Non-Newtonian Fluid Mech.*, 31(2):127–142, 1989. URL [http://dx.doi.org/10.1016/0377-0257\(89\)80027-8](http://dx.doi.org/10.1016/0377-0257(89)80027-8).
- [5] W. Zylka. Gaussian approximation and Brownian dynamics simulations for Rouse chains with hydrodynamic interaction undergoing simple shear flow. *J. Chem. Phys.*, 94(6):4628–4636, 1991. URL <http://dx.doi.org/10.1063/1.460591>.
- [6] A. Peterlin. Hydrodynamics of macromolecules in a velocity field with longitudinal gradient. *J. Poly. Sci. B, Poly. Lett.*, 4B:287–291, 1966.
- [7] R. M. Jendrejack, J. J. de Pablo, and M. D. Graham. Stochastic simulations of DNA in flow: Dynamics and the effects of hydrodynamic interactions. *J. Chem. Phys.*, 116(17):7752–7759, 2002. URL <http://dx.doi.org/10.1063/1.1466831>.
- [8] C.-C. Hsieh, L. Li, and R. G. Larson. Modeling hydrodynamic interaction in Brownian dynamics: Simulations of extensional flows of dilute solutions of DNA and polystyrene. *J. Non-Newtonian Fluid Mech.*, 113:147–191, 2003. URL [http://dx.doi.org/10.1016/S0377-0257\(03\)00107-1](http://dx.doi.org/10.1016/S0377-0257(03)00107-1).
- [9] R. Prabhakar, J. R. Prakash, and T. Sridhar. A successive fine-graining scheme for predicting the rheological properties of dilute polymer solutions. *J. Rheol.*, 48(8):1251–1278, 2004. URL <http://dx.doi.org/10.1122/1.1807841>.
- [10] P. Sunthar and J. R. Prakash. Parameter-free prediction of DNA conformations in elongational flow by Successive Fine Graining. *Macromolecules*, 38(2):617–640, 2005. URL <http://dx.doi.org/10.1021/ma0359411>.
- [11] P. Sunthar, D. A. Nguyen, R. Dubbelboer, J. R. Prakash, and T. Sridhar. Measurement and prediction of the elongational stress growth in a dilute solution of DNA molecules. *Macromolecules*, 38:10200–10209, 2005. URL <http://dx.doi.org/10.1021/ma0511907>.
- [12] R. M. Jendrejack, M. D. Graham, and J. J. de Pablo. Hydrodynamic interactions in long chain polymers: Application of the Chebyshev polynomial approximation in stochastic simulations. *J. Chem. Phys.*, 113(7):2894–2900, 2000. URL <http://dx.doi.org/10.1063/1.1305884>.
- [13] L. E. Wedgewood and H. C. Öttinger. A model of dilute polymer solutions with hydrodynamic interaction and finite extensibility. II. Shear flows. *J. Non-Newtonian Fluid Mech.*, 27:245–264, 1988. URL [http://dx.doi.org/10.1016/0377-0257\(88\)85016-X](http://dx.doi.org/10.1016/0377-0257(88)85016-X).
- [14] A. J. Kisbaugh and A. J. McHugh. A discussion of shear-thickening in bead-spring models. *J. Non-Newtonian Fluid Mech.*, 34:181–206, 1990. URL [http://dx.doi.org/10.1016/0377-0257\(90\)80017-T](http://dx.doi.org/10.1016/0377-0257(90)80017-T).
- [15] J. R. Prakash and H. C. Öttinger. Viscometric functions for a dilute solution of polymers in a good solvent. *Macromolecules*, 32(6):2028–2043, 1999. URL <http://dx.doi.org/10.1021/ma981534b>.
- [16] R. B. Bird, C. F. Curtiss, R. C. Armstrong, and O. Hassager. *Dynamics of Polymeric Liquids - Volume 2: Kinetic Theory*. John Wiley, New York, 2nd edition, 1987.
- [17] H. R. Warner. Kinetic theory and rheology of dilute suspensions of finitely extensible dumbbells. *Ind. Eng. Chem. Fundam.*, 11:379–387, 1972. URL <http://dx.doi.org/10.1021/i160043a017>.

- [18] P. E. Rouse. A theory of the linear viscoelastic properties of dilute polymer solutions of coiling polymers. *J. Chem. Phys.*, 21(7):1272–1280, 1953. URL <http://dx.doi.org/10.1063/1.1699180>.
- [19] J. G. Kirkwood and J. Riseman. The intrinsic viscosities and diffusion constants of flexible macromolecules in solution. *J. Chem. Phys.*, 16(6):565–573, 1948. URL <http://dx.doi.org/10.1063/1.1746947>.
- [20] B. H. Zimm. Chain molecule hydrodynamics by the Monte-Carlo method and the validity of the Kirkwood-Riseman approximation. *Macromolecules*, 13(3):592–602, 1980. URL <http://dx.doi.org/10.1021/ma60075a022>.
- [21] J. Rotne and S. Prager. Variational treatment of hydrodynamic interaction in polymers. *J. Chem. Phys.*, 50:4831–4837, 1969. URL <http://dx.doi.org/10.1063/1.1670977>.
- [22] H. Yamakawa. *Modern Theory of Polymer Solutions*. Harper and Row, New York, 1971.
- [23] J. M. Wiest. Birefringence in strong flows of polymer solutions. *Polymer*, 40:1917–1922, 1999. URL [http://dx.doi.org/10.1016/S0032-3861\(98\)00427-3](http://dx.doi.org/10.1016/S0032-3861(98)00427-3).
- [24] M. Doi and S. F. Edwards. *The Theory of Polymer Dynamics*. Oxford University Press, New York, 1986.
- [25] R. B. Bird, R. C. Armstrong, and O. Hassager. *Dynamics of Polymeric Liquids - Volume 1: Fluid Mechanics*. John Wiley, New York, 2nd edition, 1987.
- [26] R. Prabhakar and J. R. Prakash. Viscometric functions for Hookean dumbbells with excluded volume and hydrodynamic interaction. *J. Rheol.*, 46(5):1191–1220, 2002. URL <http://dx.doi.org/10.1122/1.1501924>.
- [27] R. Prabhakar. *Predicting the rheological properties of dilute polymer solutions using bead-spring models: Brownian dynamics simulations and closure approximations*. PhD thesis, Monash University, 2005. URL [http://users.monash.edu.au/~rprakash/thesis/Prabhakar\\_thesis.pdf](http://users.monash.edu.au/~rprakash/thesis/Prabhakar_thesis.pdf).
- [28] J. R. Prakash. Rouse chains with excluded volume interactions: Linear viscoelasticity. *Macromolecules*, 34(10):3396–3411, 2001. URL <http://dx.doi.org/10.1021/ma0006880>.
- [29] J. R. Prakash. The influence of the range of excluded volume interactions on the linear viscoelastic properties of dilute polymer solutions. *Chem. Eng. Sci.*, 56:5555–5564, 2001. URL [http://dx.doi.org/10.1016/S0009-2509\(01\)00154-3](http://dx.doi.org/10.1016/S0009-2509(01)00154-3).
- [30] K. Satheesh Kumar and J. Ravi Prakash. Universal consequences of the presence of excluded volume interactions in dilute polymer solutions undergoing shear flow. *J. Chem. Phys.*, 121(8):3886–3897, 2004. URL <http://dx.doi.org/10.1063/1.1775185>.
- [31] M. Fixman. Polymer dynamics: Boson representation and excluded volume forces. *J. Chem. Phys.*, 45(3):785–792, 1966. URL <http://dx.doi.org/10.1063/1.1727682>.
- [32] R. B. Bird, P. J. Dotson, and N. L. Johnson. Polymer solution rheology based on a finitely extensible bead-spring chain model. *J. Non-Newtonian Fluid Mech.*, 7:213–235, 1980. URL [http://dx.doi.org/10.1016/0377-0257\(80\)85007-5](http://dx.doi.org/10.1016/0377-0257(80)85007-5).
- [33] L. E. Wedgewood and R. B. Bird. From molecular models to the solution of flow problems. *Ind. Eng. Chem. Res.*, 27:1313–1320, 1988.
- [34] J. M. Wiest and R. I. Tanner. Rheology of bead-nonlinear spring chain molecules. *J. Rheol.*, 33:281–316, 1989. URL <http://dx.doi.org/10.1122/1.550060>.
- [35] J. M. Wiest, L. E. Wedgewood, and R. B. Bird. On coil-stretch transitions in dilute polymer solutions. *J. Chem. Phys.*, 90:587–594, 1989. URL <http://dx.doi.org/10.1063/1.456457>.
- [36] R. Keunings. On the Peterlin approximation for finitely extensible dumbbells. *J. Non-Newtonian Fluid Mech.*, 68:85–100, 1997. URL [http://dx.doi.org/10.1016/S0377-0257\(96\)01497-8](http://dx.doi.org/10.1016/S0377-0257(96)01497-8).
- [37] M. Herrchen and H. C. Öttinger. A detailed comparison of various FENE models. *J. Non-Newtonian Fluid Mech.*, 68:17–42, 1997. URL [http://dx.doi.org/10.1016/S0377-0257\(96\)01498-X](http://dx.doi.org/10.1016/S0377-0257(96)01498-X).
- [38] B. H. A. A. van den Brule. Brownian dynamics simulation of finitely extensible bead-spring chains. *J. Non-Newtonian Fluid Mech.*, 47:357–378, 1993. URL [http://dx.doi.org/10.1016/0377-0257\(93\)80058-J](http://dx.doi.org/10.1016/0377-0257(93)80058-J).
- [39] I. Ghosh, G. H. McKinley, R. A. Brown, and R. C. Armstrong. Deficiencies of FENE dumbbell models in describing rapid stretching of dilute polymer solutions. *J. Rheol.*, 45(3):721–758, 2001. URL <http://dx.doi.org/10.1122/1.1357822>.
- [40] G. Lielens, P. Halin, I. Jaumin, R. Keunings, and V. Legat. New closure approximations for the kinetic theory of finitely extensible dumbbells. *J. Non-Newtonian Fluid Mech.*, 76:249–279, 1998. URL [http://dx.doi.org/10.1016/S0377-0257\(97\)00121-3](http://dx.doi.org/10.1016/S0377-0257(97)00121-3).
- [41] G. Lielens, R. Keunings, and V. Legat. The FENE-L and FENE-LS closure approximations to the kinetic theory of finitely extensible dumbbells. *J. Non-Newtonian Fluid Mech.*, 87:179–196, 1999. URL [http://dx.doi.org/10.1016/S0377-0257\(99\)00063-4](http://dx.doi.org/10.1016/S0377-0257(99)00063-4).
- [42] R. Sizaire, G. Lielens, I. Jaumin, R. Keunings, and V. Legat. On the hysteretic behaviour of dilute polymer solutions in relaxation following extensional flow. *J. Non-Newtonian Fluid Mech.*, 82:233–253, 1999. URL [http://dx.doi.org/10.1016/S0377-0257\(98\)00164-5](http://dx.doi.org/10.1016/S0377-0257(98)00164-5).
- [43] A. N. Gorban, I. V. Karlin, P. Ilg, and H. C. Öttinger. Corrections and enhancements of quasi-equilibrium states. *J. Non-Newtonian Fluid Mech.*, 96:203–219, 2001. URL [http://dx.doi.org/10.1016/S0377-0257\(00\)00135-X](http://dx.doi.org/10.1016/S0377-0257(00)00135-X).
- [44] J. R. Prakash and H. C. Öttinger. Universal viscometric functions for dilute polymer solutions. *J. Non-Newtonian Fluid Mech.*, 71:245–272, 1997. URL [http://dx.doi.org/10.1016/S0377-0257\(97\)00012-8](http://dx.doi.org/10.1016/S0377-0257(97)00012-8).
- [45] M. Somasi, B. Khomami, N. J. Woo, J. S. Hur, and E. S. G. Shaqfeh. Brownian dynamics simulations of bead-rod and bead-spring chains: Numerical algorithms and coarse graining issues. *J. Non-Newtonian Fluid Mech.*, 108:227–255, 2002. URL [http://dx.doi.org/10.1016/S0377-0257\(02\)00132-5](http://dx.doi.org/10.1016/S0377-0257(02)00132-5).
- [46] R. Prabhakar and J. R. Prakash. Multiplicative separation of the influences of excluded volume, hydrodynamic interactions and finite extensibility on the rheological properties of dilute polymer solutions. *J. Non-Newtonian Fluid Mech.*, 116(2-3):163–182, 2004. URL [http://dx.doi.org/10.1016/S0377-0257\(03\)00155-1](http://dx.doi.org/10.1016/S0377-0257(03)00155-1).
- [47] P. S. Doyle and E. S. G. Shaqfeh. Dynamic simulation of freely draining, flexible bead-rod chains: Start-up of extensional and shear flow. *J. Non-Newtonian Fluid Mech.*, 76:43–78, 1998. URL [http://dx.doi.org/10.1016/S0377-0257\(97\)00112-2](http://dx.doi.org/10.1016/S0377-0257(97)00112-2).
- [48] J. S. Hur, E. S. G. Shaqfeh, H. P. Babcock, D. E. Smith,

- and S. Chu. Dynamics of dilute and semidilute DNA solutions in the start-up of shear flow. *J. Rheol.*, 45:421–450, 2001. URL <http://dx.doi.org/10.1122/1.1339246>.
- [49] R. G. Larson. *Constitutive Equations for Polymer Melts and Solutions*. Butterworths, Boston, 1988.
- [50] H. C. Öttinger. Velocity field in nondraining polymer chains. *Rheol. Acta*, 35:134–138, 1996.
- [51] P. S. Doyle, E. S. G. Shaqfeh, G. H. McKinley, and S. H. Spiegelberg. Relaxation of dilute polymers solutions following extensional flow. *J. Non-Newtonian Fluid Mech.*, 76:79–110, 1998. URL [http://dx.doi.org/10.1016/S0377-0257\(97\)00113-4](http://dx.doi.org/10.1016/S0377-0257(97)00113-4).
- [52] S. H. Spiegelberg and G. H. McKinley. Elastic and viscous contributions to stress in extensional rheometry of viscous polymer solutions. In *Proceedings of the XIth International Congress on Rheology*, page 211–212, Quebec City, 1996.
- [53] N. V. Orr and T. Sridhar. Probing the dynamics of polymer solutions in extensional flow using step strain rate experiments. *J. Non-Newtonian Fluid Mech.*, 82:203–232, 1999. URL [http://dx.doi.org/10.1016/S0377-0257\(98\)00163-3](http://dx.doi.org/10.1016/S0377-0257(98)00163-3).
- [54] L. Li and R. G. Larson. Excluded volume effects on the birefringence and stress of dilute polymer solutions in extensional flow. *Rheol. Acta*, 39:419–427, 2000.
- [55] O. Hassager. Kinetic theory and rheology of bead-rod models for macromolecular solutions I. Equilibrium and steady flow properties. *J. Chem. Phys.*, 60(5):2111–2124, 1974. URL <http://dx.doi.org/10.1063/1.1681321>.
- [56] C. M. Schroeder, E. S. G. Shaqfeh, and S. Chu. Effect of hydrodynamic interactions on DNA dynamics in extensional flow: Simulation and single molecule experiments. *Macromolecules*, 37:9242–9256, 2004. URL <http://dx.doi.org/10.1021/ma0494611>.
- [57] P.-G. De Gennes. Coil-stretch transition of dilute flexible polymers under ultrahigh velocity gradients. *J. Chem. Phys.*, 60:5030–5042, 1974. URL <http://dx.doi.org/10.1063/1.1681018>.
- [58] X. J. Fan, R. B. Bird, and M. Renardy. Configuration-dependent friction coefficients and elastic dumbbell rheology. *J. Non-Newtonian Fluid Mech.*, 18:255–272, 1985. URL [http://dx.doi.org/10.1016/0377-0257\(85\)87002-6](http://dx.doi.org/10.1016/0377-0257(85)87002-6).
- [59] C. M. Schroeder, H. P. Babcock, E. S. G. Shaqfeh, and S. Chu. Observation of polymer conformation hysteresis in extensional flow. *Science*, 301:1515–1519, 2003.
- [60] W. Zylka and H. C. Öttinger. Calculation of various universal properties for dilute polymer solutions undergoing shear flow. *Macromolecules*, 24(2):484–494, 1991. URL <http://dx.doi.org/10.1021/ma00002a023>.

